Laser-assisted fabrication of Si biomimetic hierarchical surfaces for tissue engineering applications

Master Thesis

Sofia Bakogianni

Supervisor: Costas Fotakis

University of Crete

July 2010

Laser-assisted fabrication of Si biomimetic hierarchical surfaces for tissue engineering applications

Abstract

This dissertation deals with ultrafast laser micro/nano- structuring of crystalline silicon. Irradiation of crystalline Si with intense, ultrafast laser light in the presence of a reactive gas (sulfur hexafluoride, SF_6) or in water environment leads to a change in its surface morphology. Upon laser irradiation, silicon surface is covered with a quasi-ordered array of micrometer-sized structures (Si spikes), when processing occurs in SF_6, or with high density regular arrays of nanometer-scale structures (Si ripples, Si rods) when processing occurs in water. The microstructured Si surface has near-unity absorptance from the near-ultraviolet to the near-infrared and acquires increased hydrophobicity. Finally, we report on the potential biological applications that laser-structured Si may have. We investigate the fibroblast cell adhesion and viability on the laser-textured Si surfaces as well as the covalent attachment of amyloid peptides on them.

Acknowledgements

I would like to express my gratitude to my Professor Costas Fotakis and my supervisors Manolis Stratakis and Anthi Ranella for the guidance and assistance they provided at all levels. I would like to thank my co-students for their help and advice. A very special thanks to my family and friends for the support they provided. Finally, I would like to thank Institute of Electronic Structure and Laser (FORTH) and the Department of Physics of the University of Crete for the support.

Contents

List of Figures

Chapter 1

Introduction

Semiconductor devices are the foundation of modern electronics and include various types of transistors and solar cells, many kinds of diodes such as the light-emitting diode, as well as digital and analog integrated circuits. Dozens of semiconducting materials are exploited commercially, including the germanium (Ge) and the gallium arsenide (GaAs). Silicon (Si), though, is the most dominant material in the field of electronics and photonics. Silicon is a well-characterized material with well-defined properties, is produced in abundance and in low-cost comparatively with other semiconducting materials. It can be easily integrated in electronic circuits based on the developing CMOS technology, detect visible light and convert, directly, sunlight radiation into electrical energy. All these factors combined with its favorable electrical conductivity have constituted Si the basis of optoelectronic and microelectronic applications.

However, silicon exhibits some drawbacks as a material and its use is limited concerning specific implementations. Silicon is a poor light emitter as a semiconductor with an indirect band gap, cannot detect important communication wavelengths located in the infrared region of light spectrum and, as a solar cell, cannot convert efficiently sun's radiation into electric current due to its nearly-zero absorption for energies lower than its energy gap (1.07eV). Significant research efforts have been made in order to overcome, primarily, these limitations and extend, secondarily, the use of silicon in interdisciplinary applications.

Extensive scientific research has been conducted towards the development of new fabrication techniques, which could improve and/or extend silicon's properties. Towards this goal, a great amount of research effort has been focused on the modification of materials surface properties using intense, pulsed laser irradiation. Laser irradiation can induce the manufacture of structures on the exposed silicon surfaces both in the micrometer and nanometer length-scale. The microstructuring of silicon's surface seems to be favorably consistent with the novel subfield of electronics, microelectronics which is related to the study and fabrication of electrical devices at micrometer dimensions.

Semiconductor microdevices have splendid applications not only in photonics or electronics but also in bioelectronics which emerges at the interface of multiple scientific fields. For instance, the technology of silicon-based biomedical microdevices for implantable diagnostic and therapeutic purposes requires the synergy of electronics, biology, physics, chemistry and materials science. By spanning and integrating these diverse subject areas, it may be feasible to interact with, measure and understand biological systems, enabling advanced technology from lab-on-chip biomedical diagnoses to implantable neural interfaces.

Undoubtedly, one of the greatest challenges with silicon-based biomedical microdevices such as those developed for neural stimulation, implantable encapsulation, biosensors and drug delivery, is to improve the biocompatibility and tissue integration. This means that the biological response of inorganic materials, such as silicon's, seems to be of vital importance in the development of bioengineering. This involves the ability of tuning materials surface chemistry and microstructure and, therefore, converting them into functional biomaterials.

This thesis describes a method which induces various surface modifications (morphological, structural and compositional) on crystalline silicon and, thus, alters its surface properties. These modifications are accomplished during the action of ultrafast pulsed laser irradiation of crystalline Si wafers in the presence of a reactive gas or aqueous media. The manufactured structures possess unique micro/nano morphology and exhibit improved optical, electronic and wetting properties. [17]

This laser-based fabrication technique of silicon may eliminate certain problems faced in optoelectronics or photovoltaic technology. The potential progress arisen in such technological applications is going to be mentioned, nevertheless, this thesis focalizes in the implementation of micro/nano- structured silicon in the promising and challenging field of tissue engineering.

Content and organization

This thesis is organized as follows:

In Chapter 1 we study the morphology of the structures fabricated on Si surface at the micrometer and submicrometer length-scale upon femtosecond laser irradiation by varying the laser fluence under constant reactive gas conditions. Furthermore, we demonstrate the formation of structures at nanometer length-scale using as well different laser fluences with the fabrication process occurring in water environment. This chapter, also, reviews the basic processes taking place upon the interaction of intense laser pulses with semiconductors and discuss on the possible mechanisms for the different structures formation.

In Chapter 2 we investigate the optical properties of the laser-formed silicon structures both in reactive gas atmosphere and in water environment. We ascertain increased absorptance which can reach up to more than 90% throughout a wide spectral range (from UV to NIR). The effect of surface morphology on silicon's optical response is examined.

In Chapter 3 we study the wetting response of the laser-textured Si surfaces both in reactive gas atmosphere and in water environment. A general observation is that the initially hydrophilic surface of the flat silicon is converted into hydrophobic upon laser structuring. This is a direct consequence of the morphology of the Si structured surfaces.

In Chapter 4 we examine potential biological applications that the micro/nano-sized Si structures may have. Firstly, we investigate fibroblast cell adhesion and viability on modificated Si surfaces exhibiting gradient roughness ratios and wettabilities. Secondly, we use a bio-functionalization technique which is capable of rendering silicon's structured surface more appropriate as an interface for biological applications. The technique makes use of the formation of self-assembled monolayers (SAMs) on silicon surface by exploiting the thiol chemistry. One target is the selective attachment of an octapeptide, which belongs to the category of amyloid peptides and forms fibrils in solution, on the manufactured surfaces. The ultimate target, though, is to achieve the immobilization of bioactive peptides (RGD-peptides) on silicon substrates.

Chapter 2

Ultrafast Laser-Assisted Silicon Mico/Nano- Structuring

Laser-assisted surface processing of crystalline Si wafers has become the subject of intensive scientific and technological research for over a decade. [1] The interaction of laser irradiation with materials and, in particular with semiconductors is usually accompanied with the acquisition of different forms of the ordinary semiconducting materials. [2, 3] Si absorbs laser photons and its surface can be permanently modified through melting and resolidification, vaporization or ablation processes.

In particular, intense, ultrafast laser irradiation can cause periodic patterns in the form of ripples (known as laser-induced periodic surface structures (LIPSS) [4, 5] as well as surface structures with superior control over structure geometry and pattern regularity. These surface structures obtain conical features (spikes), as shown in Figure 2.1.

In this work, we deal with the formation of silicon structures, both at

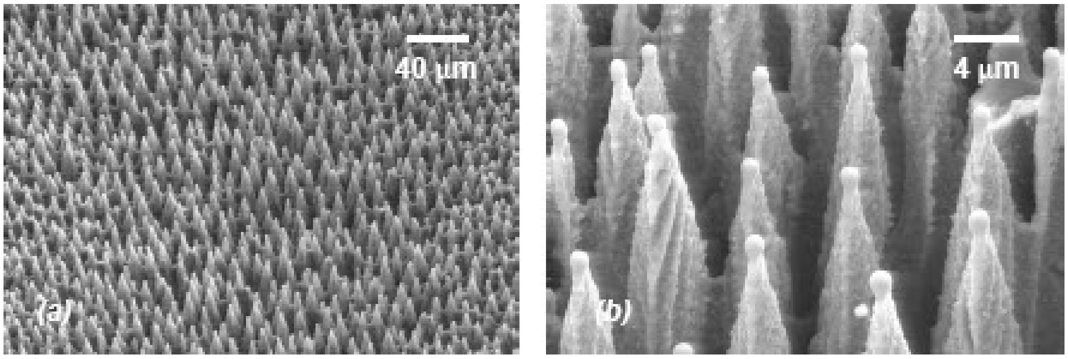

Figure 2.1: SEM micrographs of silicon spikes (a) side view, (b) close-up view.

the micrometer and the nanometer length-scales, upon laser irradiation with hundreds of femtosecond laser pulses. The processes by which femtosecond laser pulses interact with silicon differ greatly from those with picosecond or longer pulses. [6, 7] The modification of silicon with ultrafast pulses is not yet well-understood but it is considered that non-thermal, ultrafast phase transformations can occur on a timescale much faster than thermal processes. [8, 9] It is widely known, yet, that the interaction of femtosecond laser irradiation with silicon leads to the formation of conical structures on its surface, whose characteristics depend on laser and ambient gas parameters. [10] These conical structures (spikes) can be up to 10 microns tall, exhibiting protrusions on their walls at the submicrometer scale and the intra-spike separation is a few microns.

In this chapter, details on the experimental procedure of silicon surface structuring are provided. Then, the morphology of the patterned Si surfaces fabricated using a Ti:Sapphire laser source both in constant reactive gas atmosphere and in water environment is investigated. In particular, the effect of laser fluence on the morphology of the obtained structures is studied. In the last section of the chapter, the basic processes taking place upon the interaction of intense laser pulses with solids (semiconductors), as well as the proposed mechanisms behind the formation of the structures on materials surface upon laser irradiation both in reactive gas ambient and in water environment are discussed.

2.1 Ultrafast laser Si structuring in reactive gas atmosphere

2.1.1 Experimental procedure

The experimental procedure for Si surface structuring is shown in Figure 2.2. Single crystal n-type Si (100) wafers are subjected to laser irradiation in a vacuum chamber evacuated down to a residual pressure of about 10^{-2} mbar by means of a rotary pump. A micro valve system attached to the chamber enables a precise backfilling of the reactive gas (SF_6), the pressure of which is measured with a baratron gauge.

The laser beam is focused with a quartz lens on the silicon substrate mounted to a sample holder inside the vacuum processing chamber. The laser fluence is varied by using an attenuator or optical density filters. The laser beam is entered the chamber through a quartz entrance window, normal to the sample, while the irradiation process can be monitored through this window.

The processing chamber is placed on a computer driven high precision X-Y translation stage with spatial resolution of 1μm allowing sample displacement with regard to the laser beam. This system allows control over the amount of overlap between consecutive scans when large area structuring is required. The irradiating source is constituted by a regenerative amplified Ti:Sapphire (λ=800nm) delivering 200fs pulses at a repetition rate of 1kHz. The laser beam is focused with a 0.25m focal-length lens onto the sample. The lens is mounted on a translation stage to allow different spot sizes to be produced on the sample. The spot size of the nearly Gaussian laser beam is measured with a CCD camera. Typical spot sizes range from 100μm to 200μm.

Before laser processing, the Si wafers are cleaned in a 10-minute trichloroethylene, followed by a 10-minute acetone, followed by a 10-minute methanol bath. Then, laser scanning can be conducted by two ways. The first is to scan the laser beam over the sample by displacing the sample during the exposure of the laser pulses. This method allows the structuring over a large area of silicon surface. The second way requires a mechanical shutter to be synchronized to the translation stages, exposing any given spot on the Si surface to a controlled average number of pulses. This method allows the irradiation of just a single spot or of larger areas offering precise control over the number of laser pulses to which the surface is exposed and, thus, avoiding nonuniform samples.

2.1.2 Morphological analysis

In this subsection, we examine the formation of structures on Si surface upon ultrafast laser irradiation in the presence of SF_6 (sulfur hexafluoride has the role of the reactive gas). Modifications in surface morphology of Si can be achieved through varying laser parameters (laser fluence, laser wavelength, number of laser pulses, pulse duration, etc.) or reactive gas parameters (gas pressure, type of gas). In this work, the impact of laser fluence on the morphology and the geometrical characteristics of the fabricated structures is investigated.

For our experiments, each laser-structured surface is fabricated at constant laser fluence ranging from 0.17 to 2.29 J/cm^2. After laser processing, each surface is morphologically characterized by field emission scanning electron microscopy (SEM). An image processing algorithm is implemented in order to obtain quantitive information concerning the topological characteristics of the formed structures i.e. spikes' density, profile, height, and separation.

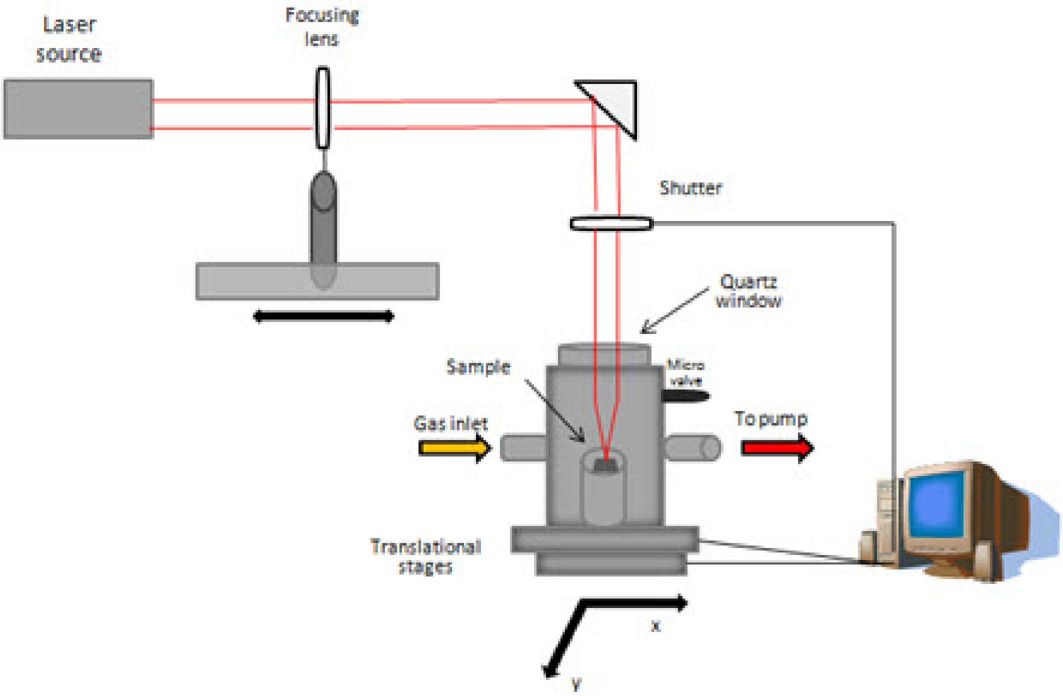

Figure 2.2: Experimental set-up of laser Si microstructuring in reactive gas atmosphere (SF_6.

Laser fluence dependence

As depicted in the SEM micrographs of the patterned Si surfaces produced at different laser energies per unit area (Figure 2.3), the textured areas comprise forests of conical microstructures (spikes). In all cases, Si spikes are fabricated at constant gas pressure (SF_6 at 500 Torr) by exposing any given spot on the Si surface to an average of 500 pulses.

Variations of laser fluence cause remarkable changes in the structures as to dimension and density. By increasing laser fluence, conical microstructuring is promoted on the Si surface, with structures becoming more pronounced and spatially separated. Besides directly affecting the micrometer length-scale surface topography, increasing fluence is also crucial to induce a more pronounced submicrometer decoration on the spikes' walls.

In particular, spikes' height varies from one to ten micrometers (Figure 2.4), while the size of the protrusions on Si cones ranges from tens to a few hundred of nanometers, providing a double length-scale pattern on silicon surface.

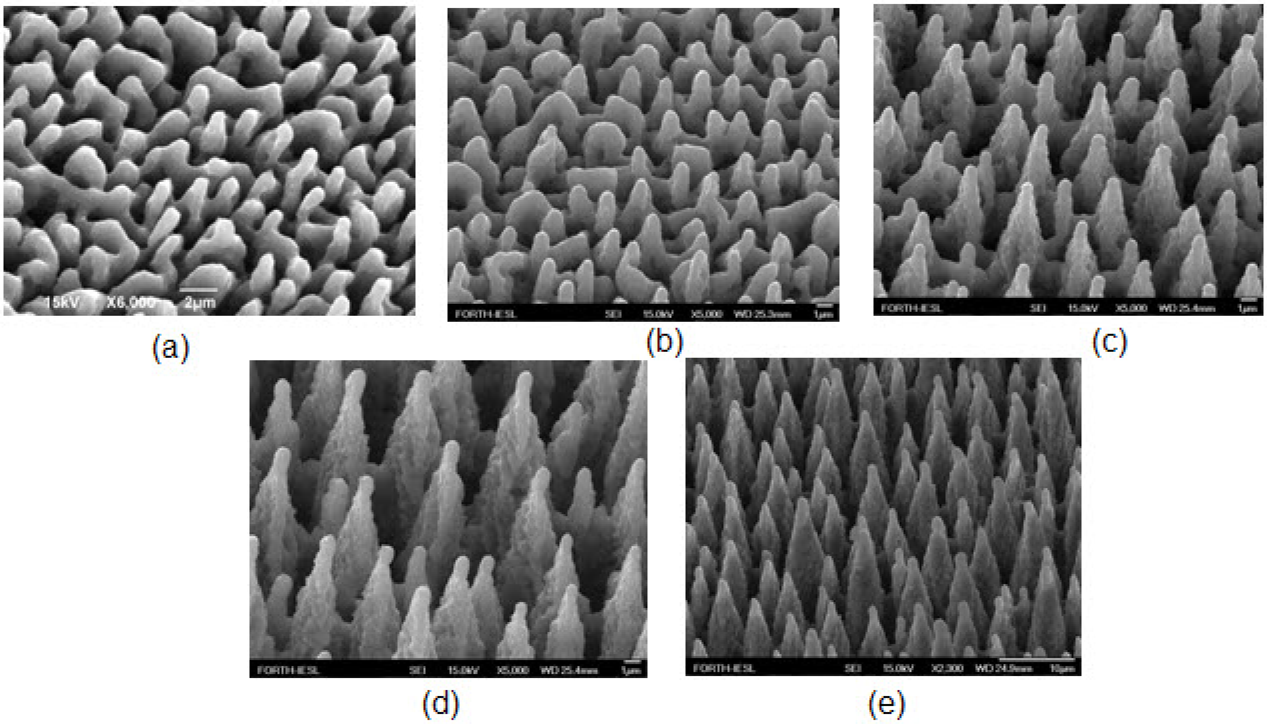

(a) (b) (c)

(d) (e)

Figure 2.3: Side-view SEM micrographs of silicon spikes fabricated at fluence: (a) 0.17 J/cm^2, (b) 0.34 J/cm^2, (c) 0.68 J/cm^2, (d) 1.15 J/cm^2 and (e) 2.29 J/cm^2.

As shown in the next graph, spikes' density decreases with increasing laser fluence and its value ranges from 10^6 to $10^7/cm^2$ (Figure 2.5), whereas, intra-spike seperation increases with increasing laser fluence ranging from about 1 to 6 micrometers.

Finally, it should be outlined that the reactive gas also plays a distinct role in the fabrication process, since it determines the sharpness of the structures obtained. The Si structures fabricated in vacuum are blunt and irregular (Figure 2.6 (a)). However they become more pronounced with increasing ambient gas pressure (250-1250 Torr). Increasing reactive gas pressure, as laser fluence and number of pulses, acts favorably to the formation of second-length scale roughness on the surface of the cones (Figure 2.6 (b)). [27]

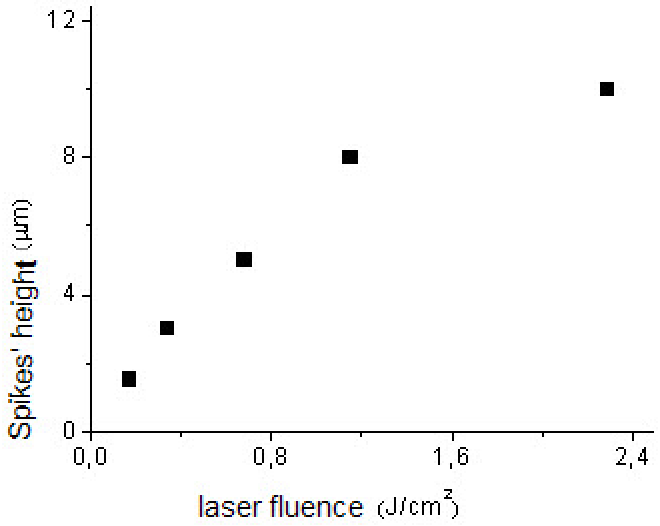

Figure 2.4: Laser fluence dependence of spike's height.

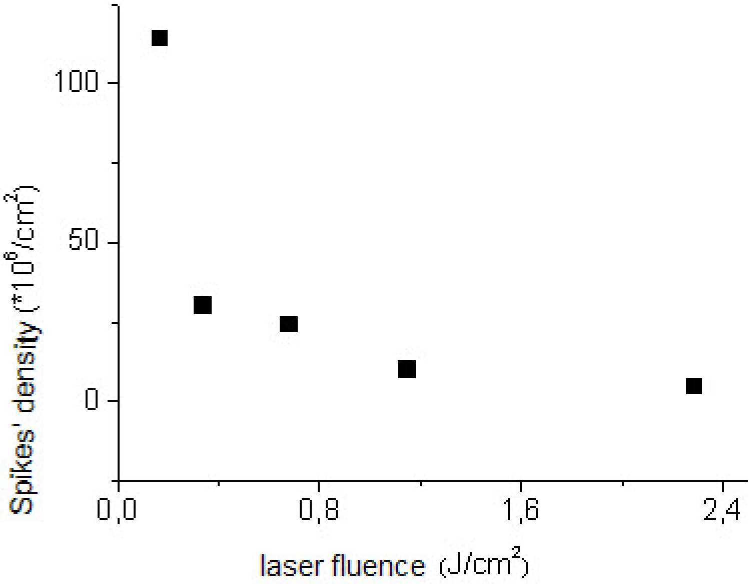

Figure 2.5: Laser fluence dependence of spike's density.

2.1.3 Structural and compositional analysis

The formed structures consist of a core of undisturbed Si covered with a few hundred nanometer thick, highly disordered layer. The disordered layer covering the Si cones extends from their tips down to their bases, while no interface can be distinguished between the Si substrate and the Si cones. It

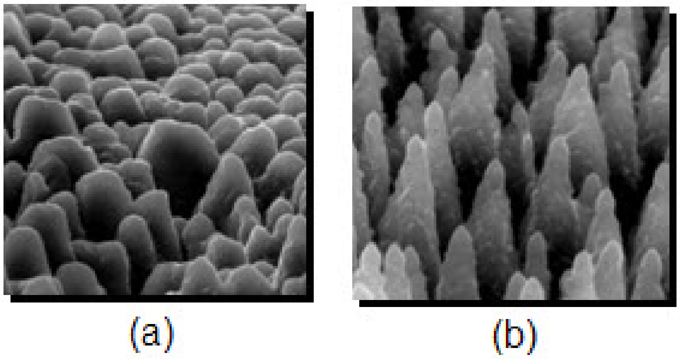
(a) (b)

Figure 2.6: Side SEM images of Si microstructures fabricated in (a) vacuum, (b) a 500 Torr SF_6 atmosphere.

is evident that the interior of the spikes is single crystalline independently of the laser parameters. Moreover, since the Si substrate is also oriented along the [100] crystallographic axis, the spikes obtain the same orientation as the substrate that they are grown on. [27]

The composition of both the disordered outer layer, as well as the interior of the fabricated micro-cones has been determined. [27] The surface layer contains sulphur (S), a result of the photodissociation of SF_6, at a concentration of the order of 1 wt%. However no sulphur is detected in the spikes interior. Furthermore, silicon oxide exists on the surface of the cones. [27]

2.2 Ultrafast laser Si structuring in water environment

As described in section 2.1, the patterned Si surfaces produced at different laser energies per unit area (fluences), in the presence of reactive gas (SF_6) comprise forests of conical structures (spikes) exhibiting features at the micrometer and submicrometer length-scale. Variations of laser fluence cause remarkable changes in spikes topology. Besides affecting the micrometer-scale topology, increasing fluence is also crucial to induce a more pronounced submicrometer decoration on spikes' walls. In particular, spikes' height varies from one to ten micrometers, while the size of wall-protrusions is mainly at the scale of a few hundred of nanometers, providing a double length-scale pattern on the silicon surface. The micrometer-scale features, together with the submicrometer scale structures result into the enhancement of the overall roughness.

Mazur et al. have directed towards the formation of smaller feature sizes on Si surface. They have reported the formation of high-density regular arrays of nanometer-scale structures using femtosecond laser irradiation of a silicon surface immersed in water. The resulting surfaces exhibit nanometer-scale ripples or nanometer-scale rods depending on the laser-based procedure. [28]

In this section, the formation of nanometer-scale features using femtosecond laser irradiation of a silicon surface immersed in water is investigated. We use 800nm femtosecond irradiation, below the ablation threshold, and the resulting Si surfaces exhibit structures at the nanometer length-scale.

2.2.1 Experimental procedure

A single crystalline n-type silicon wafer (100) or a micro-patterned silicon substrate is placed in a glass container filled with distilled water, which is then mounted on the translation stages. The sample is irradiated by 1kHz train of 200fs, 800nm laser pulses from an amplified Ti:Sapphire laser source. The laser pulses are focused by a 0.25m focal length lens. The focal point is approximately located behind the substrate surface, and the spatial profile of the laser spot is nearly Gaussian. The sample is translated in a direction perpendicular to the laser beam. The experimental set-up is shown in Figure 2.7

The silicon substrate is exposed to a one-step procedure in order to create nanometer-scale ripples and to a two-step procedure in order to create nanometer-scale rods onto the surface. The laser pulses travel through approximately 10mm of water before striking the Si surface at normal incidence. The sample is irradiated, in the water environment, at low fluence regime. SEM images reveal the structures formed on the laser-textured silicon substrates.

2.2.2 Morphological analysis

In this section, we examine the formation of nanometer-scale structures on Si surface upon ultrafast laser irradiation in water environment. The impact of laser fluence on the morphology of the fabricated structures is investigated. Our experiments are performed in a low fluence regime. Then each surface is morphologically characterized by field emission scanning electron microscopy (SEM).

Firstly, a crystalline Si wafer is irradiated in water under constant laser

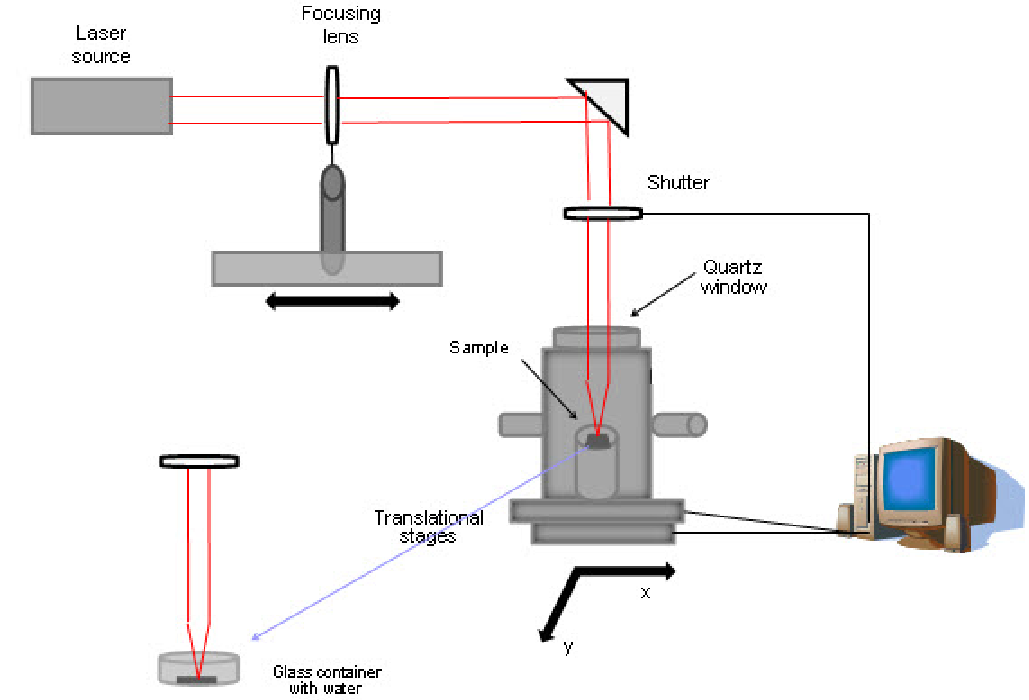

Figure 2.7: Experimental set-up of laser Si nanostructuring in water environment.

fluence (0.08 J/cm^2) by varying the number of the incident laser pulses (Figure 2.8). We can, therefore, examine the dynamic evolution of the surface topology in correlation with the number of the laser pulses. After a few laser pulses (4 to 10 pulses), overlapping spherical waves are observed on the surface, probably due to surface defects. By increasing the number of pulses (15-100 pulses), straight ripples are formed whose pattern becomes more distinct with higher number of incident pulses (200-300 pulses). Further increase in pulse shots may destroy the Si distinct pattern.

Scanning the laser beam onto the Si surface within the water, larger samples can be structured maintaining the low laser fluence regime. As it is illustrated in Figure 2.9(b), straight ripples form with spacing of about 120nm and width of about 55nm. The long axis of the ripples is perpendicular to the laser polarization. Further increase in laser fluence may lead to the formation of grooves which are parallel to laser polarization and perpendicular to the long axis of the ripples. For fluences below 0.05 J/cm^2, no formation of ripples is observed.

If the ripples, formed under the low fluence regime, are irradiated a second time in water at a fluence of 0.05J/cm^2 with the laser polarization ro-

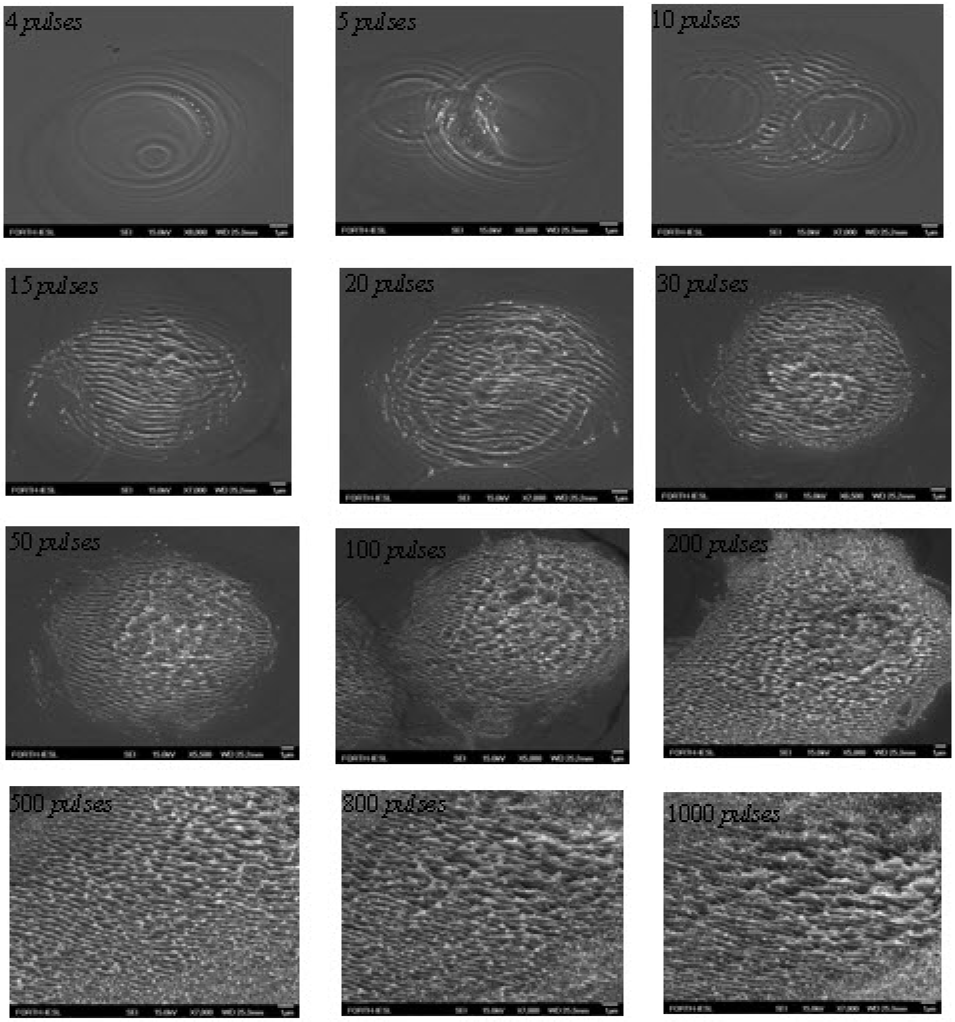

Figure 2.8: Scanning electron micrographs of a silicon surface irradiated in distilled water by an increasing number of laser pulses. Irradiation is perfomed using a 800nm/200fs pulsed laser at a fluence of 0.1J/cm^2.

tated by 90^o so that it becomes parallel with the long axis of the ripples, the ripples break up into the nanometer-scale rods shown in Figure 2.10. This two-step irradiation process results in a surface that is uniformly covered with nanometer-scale rods.

The Si nanorods are about 60nm in diameter with a spacing of less than 60nm and can be up to a few hundreds of nanometers tall, protruding normal to the surface (Figure 2.11. The density if the nanorods is quite high and can reach the value of $5.5*10^9/cm^2$

Additionally, we examine the impact of substrate surface roughness on

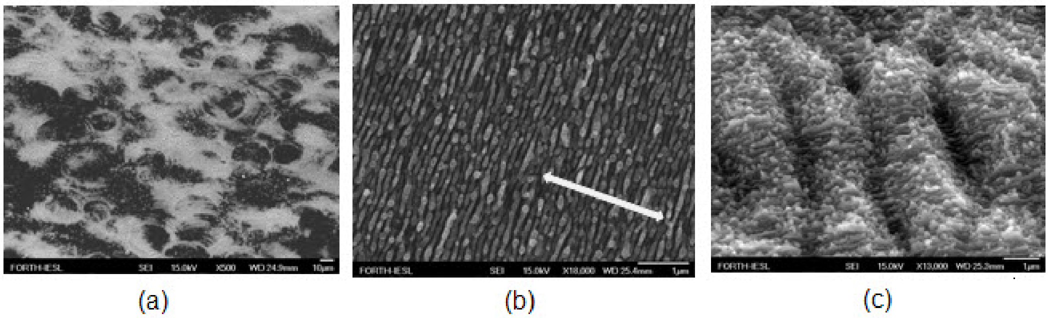
(a) (b) (c)

Figure 2.9: (a) SEM picture of silicon surfaces after irradiation in water with 800nm/200fs laser pulses with an average of 500 pulses at fluence: (a) 0.05J/cm^2, (b) 0.1J/cm^2 and (c) 0.5J/cm^2. The arrow indicates the direction of the laser polarization.

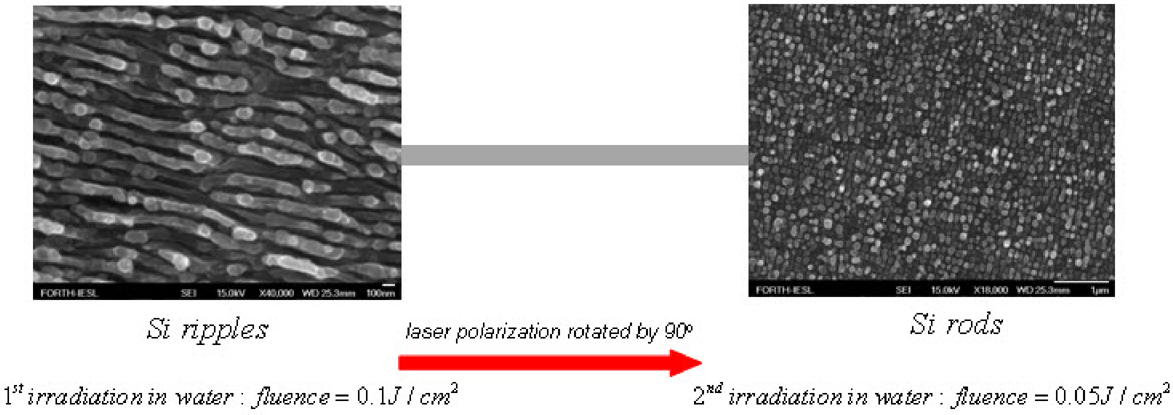

Figure 2.10: Formation process of nanometer-scale rods.

nanometer-scale ripple and rod formation. Surface roughness is induced by irradiating a flat silicon substrate in the presence of SF_6 to structure micrometer-sized spikes at different laser fluences (section 2.1). We, then, expose the microstructured substrates to the irradiation process taking place in water in order to create the nanometer-scale features.

Firstly, we investigate the value of laser fluence required for the ripple formation onto the microstructured Si. We observe that for each microstructured substrate different values of laser fluence are needed in order to form straight ripples. We use,initially, three microstructured substrates belonging to different fluence regimes (low, mid and high) and then we apply the irradiation process in water. Figure 2.12 (microstructuring at low fluence), Figure 2.13

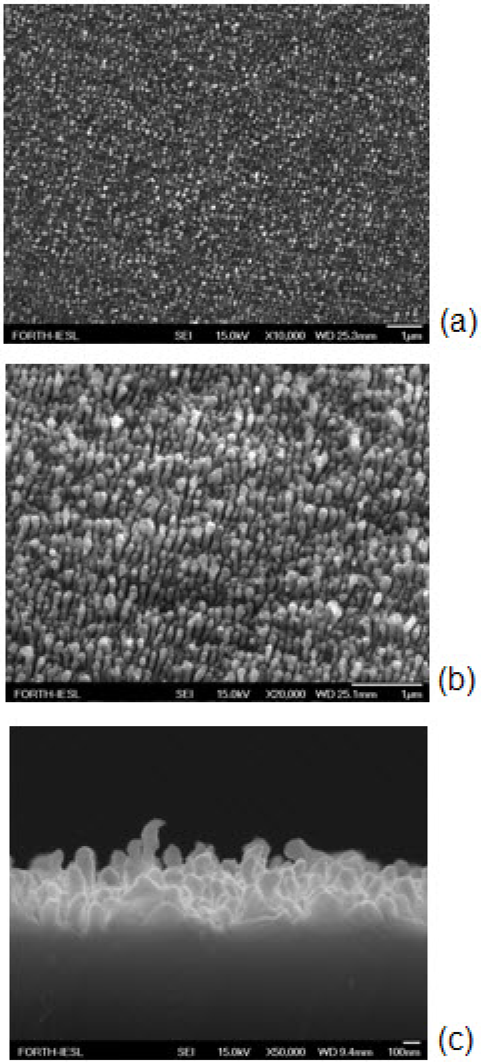

Figure 2.11: SEM picture of nanometer-scale rods formed using a two-step irradiation process of a silicon surface. (a)Top view, (b) side-view, and (c) cross-sectional side view of the nanometer-scale rods.

(microstructuring at medium fluence) and Figure 2.14 (microstructuring at high fluence) present the results obtained.

Specifically, we observe that each microstructured sample needs different laser fluence in order to form straight ripples on its cones. For microstructuring at high fluence, higher value of laser fluence is required for the irradiation occuring in water. We know that by increasing laser fluence, in the presence of SF_6, protrusions at the submicrometer length-scale are formed on spikes' walls. Consequently, the microsized cones need higher fluence, for the irradi-

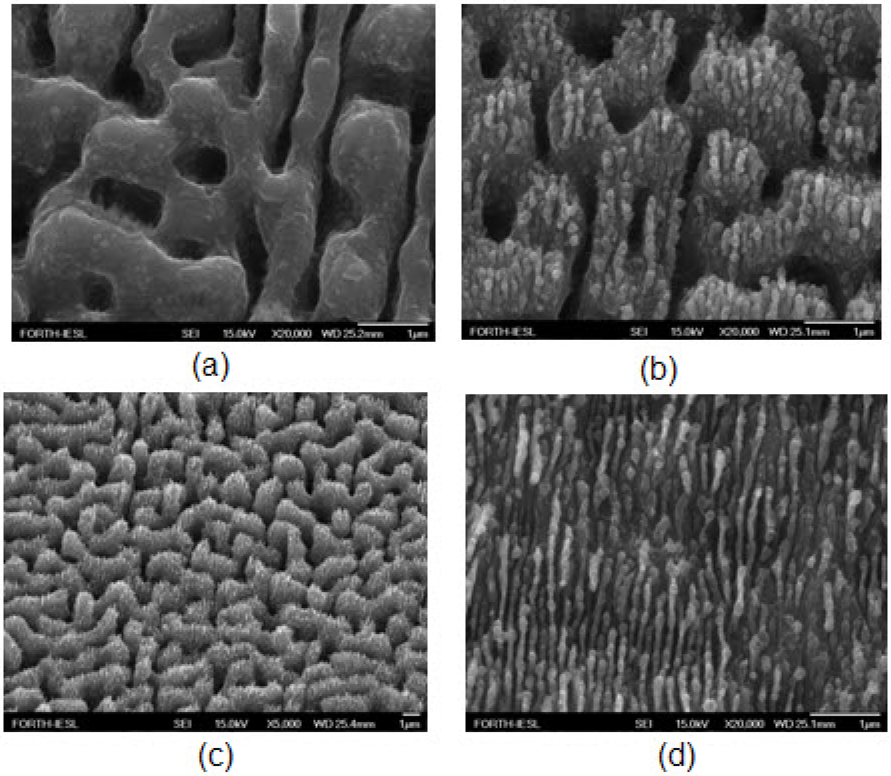

Figure 2.12: SEM pictures of nanometer-scale ripples formed on a microstructured silicon surface. (a) Initial microstructured Si surface produced at fluence: 0.16J/cm^2. Irradiation of the microstructured substrate (shown in (a)) in water at fluence: (b) 0.07J/cm^2, (c) 0.1J/cm^2 and (d) 0.2J/cm^2

ation process in water, in order to melt,initially, their protrusions and then form the straight ripples on them.

Another significant observation is that if the laser fluence exceeds a value (this value depends on the microstructured substrate) the underlying structures can be destroyed (Figure 2.12 (d)) . However, straight ripples are formed in that case as well.

Finally, as soon as, straight ripples are formed on the microstructured samples, the substrates are irradiated for a second time in water at a very low flunece of 0.05J/cm^2, with the laser polarization rotated by 90^o so that it becomes parallel with the long axis of the ripples. The ripples break up into the nanometer-scale rods shown in Figure 2.15. A three step irradiation process is required, therefore, for the rod formation onto the surface of Si spikes.

Before completing this section, it is important to outline the advantage that the laser processing in water offers concerning the surface topology. Al-

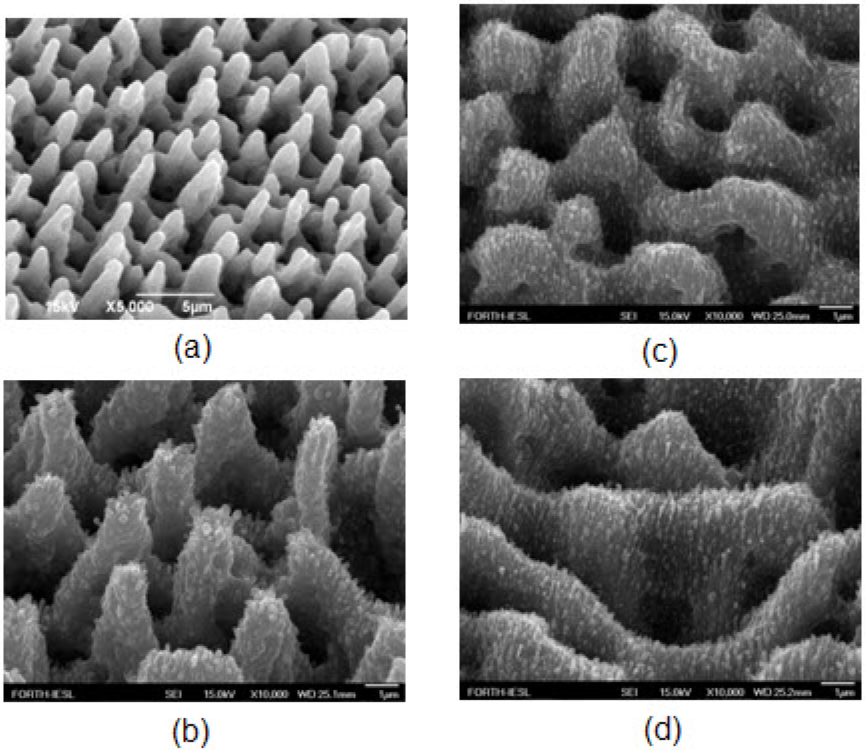

(a) (c)

(b) (d)

Figure 2.13: SEM pictures of nanometer-scale ripples formed on a microstructured silicon surface. (a) Initial microstructured Si surface produced at fluence: 0.34J/cm^2. Irradiation of the microstructured substrate (shown in (a)) in water at fluence: (b) 0.1J/cm^2, (c) 0.2J/cm^2 and (d) 0.3J/cm^2

though, laser structuring in water requires two irradiation steps in order to cover the micro-sized spikes with nanometer-scale features, these features can be fabricated in a reproducible and, mainly, controlled way. In contrast, the protrusions that are formed on spikes' walls during laser processing in the presence of a reactive gas, are at the submicrometer length-scale and are formed spontaneously. Such irradiation process lacks of control over the nanometer-scale features.

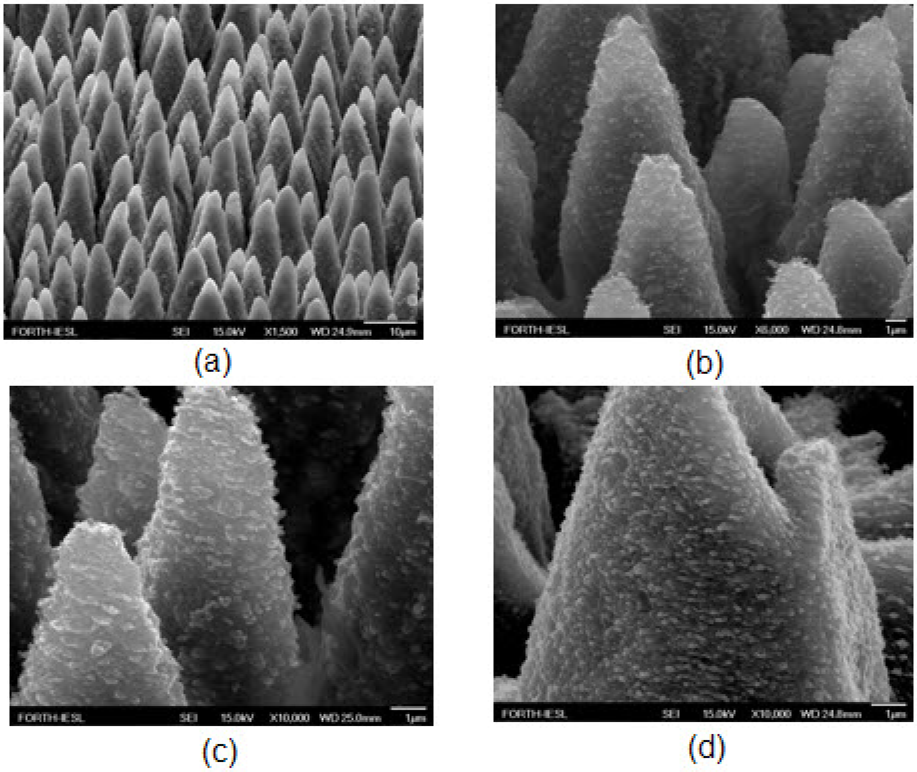

Figure 2.14: SEM pictures of nanometer-scale ripples formed on a microstructured silicon surface. (a) Initial microstructured Si surface produced at fluence: 1.15J/cm^2. Irradiation of the microstructured substrate (shown in (a)) in water at fluence: (b) 0.07J/cm^2, (c) 0.1J/cm^2 and (d) 0.5J/cm^2

2.3 Femtosecond laser-semiconductor interactions

2.3.1 Fundamental processes

When semiconducting material absorbs energetic photons from laser irradiation, its electrons are excited from their equilibrium states into higher-lying unoccupied states. This is the initial interaction of laser light with the semiconductor. Following the optical excitation, four basic processes occur. These processes are illustrated in Figure 2.16.

The electrons can undergo interband transitions by (a) single-photon excitation, (b) multi-photon excitation, (c) intraband transitions by free-carrier excitation, or (d) impact ionization. Single photon band-to band excitation is

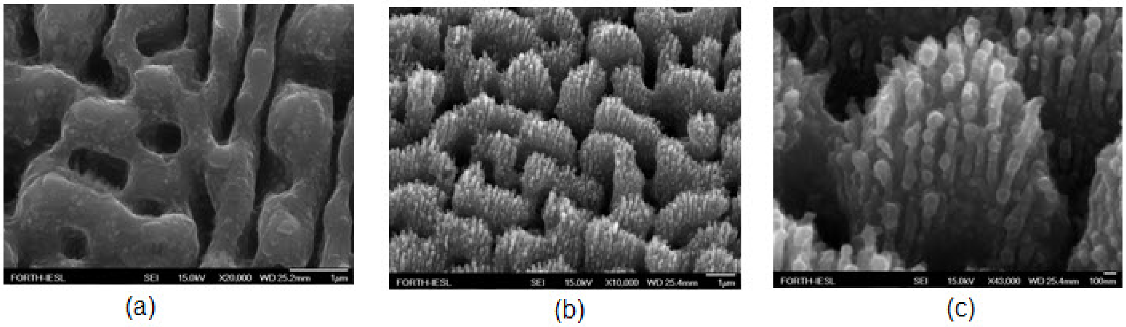

(a) (b) (c)

Figure 2.15: SEM picture of nanometer-scale rods formed on a microstructured silicon surface using a three step irradiation process (a) initial microstructured Si surface produced at fluence: 0.05J/cm^2, (b) irradiation of the surface shown in (a) in water at fluence: 0.1J/cm^2 for ripple formation, (c) irradiation of the rippled, microstructured substrate (shown in (b)) in water at fluence: 0.05J/cm^2 for rod formation

the primary process whereas the multi-photon excitation becomes increasingly significant with laser intensity, as the probability of nonlinear absorption is accordingly increased. [12] Free carrier excitation refers to the linear absorption of photons by a conduction band electron and then occupying higher states within the conduction band. If the carrier density is sufficient in the conduction band, some free carriers can acquire enough energy to create additional conduction band electrons by impact ionization.

A highly excited electron in the conduction band relaxes by releasing part of its energy through promoting another electron from the valence band to the conduction band. This process increases the density of free electrons in the conduction band. If the laser intensity is high enough, multi-photon absorption and impact ionization can lead to optical breakdown, which produces plasma. [13]

The excited electrons relax and the deposited energy is redistributed through a number of processes which lead to the structural modification of the semiconducting material. The timescales of this chain of events can be crudely classified as depicted in Figure 2.17. [12]

The primary electronic excitation is associated with very short-lived coherent polarization of the material. Dephasing processes destroy the polarization roughly on a time scale of about 10^{-14} sec. [14] The initial distribution of excited electronic states is rapidly changed by carrier-carrier interaction processes, and a quasi-equilibrium situation is established among the electrons on a time scale of about 10^{-13} sec. The quasi equilibrium electrons cool down on a timescale of 10^{-13} to 10^{-12} sec by emission of phonons (carrier-phonon

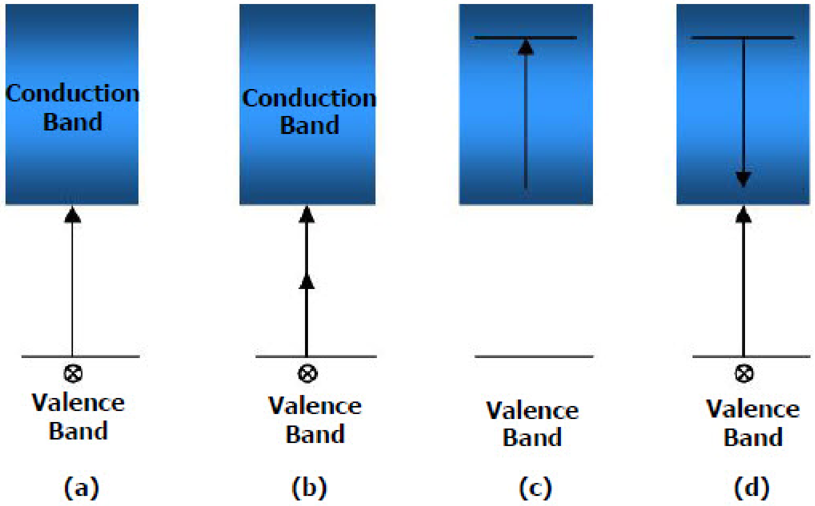

Figure 2.16: Schematic of electronic excitation in a semiconductor by laser pulses: (a) single photon excitation, (b) multi-photon excitation, (c) free carrier-absorption, (d) impact ionization

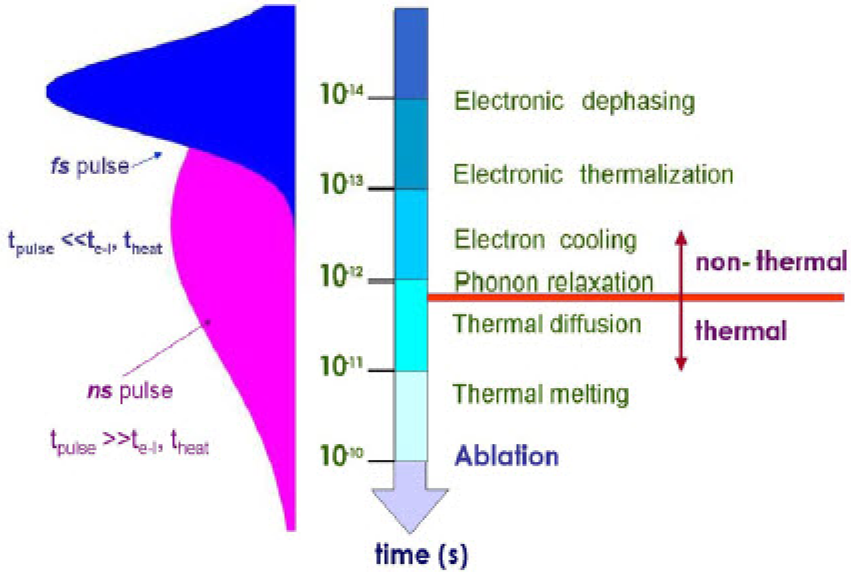

Figure 2.17: Timescales of the various secondary processes in comparison to the pulse duration at FWHM in the case of ns and fs pulses

scattering).

The final stage of the thermalization process is the redistribution of the phonons over the entire Brillouin zone according to a Bose-Einstein distribution. At this point the temperature of the laser excited material can be defined, and the energy distribution is characterized by the temperature. Subsequent processes are of thermal nature. After phonon relaxation and phonon redistribution, the diffusion of heat from the surface to the bulk, follows on the time scale of 10^{-11} sec. If the laser pulse intensity exceeds the melting threshold, melting occurs. Finally, thermal ablation takes place on a timescale of10^{-10} sec.

There is a distinct dividing line at about 10^{-12} sec defining the regime between non-thermal and thermal processes. Mechanisms leading to structural modifications using picosecond and longer laser pulses are in most cases thermal, i.e., they take place on timescales longer than a picosecond. On the other hand, employment of ultra short (femtosecond) pulses leads to a different kind of modification. As illustrated in Figure 2.17, when the pulse duration is significantly less than electron-to-lattice (ions) energy transfer time (and subsequently to the heat conduction time), non-thermal pathways may be accessed that take place on a timescale shorter than a picosecond, hence before thermal processes kick in. However, there are still several aspects of femtosecond laser induced modification of solids yet to be interpreted.

2.3.2 Laser induced periodic structures

Laser-Induced Periodic Surface Structures (LIPSS) is a form of laser induced surface modification which appears to be spatially periodic in nature, and which occurs on a wide range of both opaque and transparent materials. [3] The common morphological characteristics found in semiconductors, metals and dielectrics have led to the conclusion that the formation of laser-induced periodic surface structures by a single laser beam is a universal phenomenon that can appear on a material absorbing radiation, regardless of its dielectric constant. [3, 24]

Structures developed on solid structures can be classified into coherent and non-coherent. [17] Coherent structures are strongly related to the laser light parameters such as coherence, wavelength and polarization. The spatial periods of such structures are proportional to the laser wavelength and they are oriented perpendicularly to the electric vector of the incident light. On the other hand, the period of non-coherent structures are related to the laser-beam intensity and the ambient gas pressure, when such is used, and it is not associated with the laser wavelength and polarization. Non-coherent structures exhibit a wave-like topography with a spatial period much larger than the incident laser wavelength and appear at high laser intensities. [25] The formation of such periodic structures has been attributed to capillary waves. [26]

This initial wave-like pattern acts as a precursor to the development of Si micro-structures. Subsequent laser induced preferential material removal as well as chemical etching of the Si surface (by the reactive gas), promote conical feature formation on the Si surface. Since complex deformation mechanisms take place during the formation of Si structures, their exact role and distribution is not easy to identify. In the following sections we review on the basic characteristics of each process, by treating them separately.

Capillary waves

Surface melting upon laser irradiation may lead to the excitation of convective fluxes within the liquid layer. In laser-assisted material processing, such convective fluxes play an important role in material transport and they may originate either from changes in material density related to temperature gradients in the z- direction or from surface tensions effects. [17] In laser material processing, surface tension effects are mostly dominant since the molten layer depth, h_l, is smaller than the capillary length (l_c), i.e. $h_l < l_c = (\sigma/\rho\ g)^{1/2}$, where σ is the surface tension coefficient of the air/liquid interface, ρ is the density of the liquid and g is the gravitational acceleration. [1]

Capillary waves can be excited at the air/liquid interface when the dominant restoring force is provided by surface tension. This occurs if the above condition is met at laser fluences close to the material melting threshold. If the decay of the capillary wave activity is not complete by the time the surface resolidifies, a permanent record of the wave-like structures is frozen onto the surface (Figure 2.18). [3] The wavelength of the capillary wave is given by :

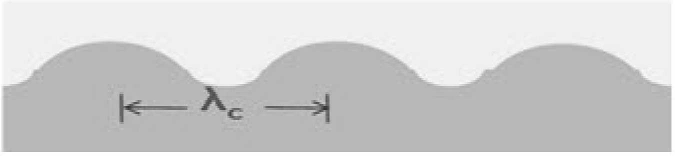

Figure 2.18: Capillary waves excited on a material surface. λ_c is the wavelength of the capillary waves. [27]

$$\lambda_c = [\frac{\sigma \cdot h}{\rho}]^{1/4} \tag{2.1}$$

where τ_c is the period of the capillary wave.

Preferential material removal

Growth of high roughness conical silicon structures from the initial wave-like pattern has been attributed to the preferential material removal, owing to further laser interaction with the semiconductor. The increase of reflectivity of the silicon surface with the increase of the incident angle may lead to the formation of silicon micro-structures. [15, 16] This results in material removal, mainly, in those areas of the material surface that are oriented normally to the laser beam axis.

In addition, the laser irradiation reflected from the silicon cone slopes can lead to light entrapment between the micro-structures, where the laser fluence is locally increased (Figure 2.19).

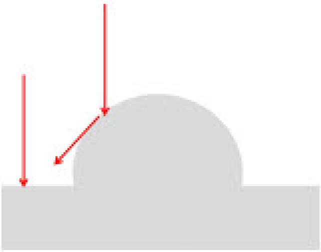

Figure 2.19: Schematic of light reflection off a protrusion leading to enhanced light absorption in the intercone areas

Laser induced chemical etching

Chemical etching can be initiated or enhanced by laser excitation of the silicon substrate, adsorbates on the surface, or species in the gas phase. Laser-chemical etching is a method of material modification, inducing either an overall change in the chemical composition of the material or the activation of real chemical reaction. [17] SF_6 is a known etchant of silicon as it is a halogen-containing gas.

SF_6 is stable at 300K and does not chemisorb on silicon. However, heating at 1000 °C is possible to initiate thermal reaction. SF_6 can be physisorbed at 90K or at a pressure of P$\geq$1 Torr at room temperature. In plasma etching applications, the dissociation of SF_6 and the resulting formation of fluorine radicals are well-known. [18, 19] Etching of silicon can then be associated with the formation of fluorine radicals, which react with silicon and, eventually, volatile Si containing fluorine compounds are formed.

Laser-induced etching of silicon with SF_6 can take place via a vibrationally or electronically excited molecule or a radical created by photodissociation. The course of the latter interaction has been studied using CO_2 laser pulses in the presence of SF_6 at normal incidence to the Si substrate. It has been suggested that gaseous or physisorbed SF_6 molecules are excited into higher vibrational states via coherent multiphoton excitation. In contrast to ground-state SF_6, vibrationally excited SF_6 can dissociatively chemisorb on Si surfaces resulting to the formation of fluorine ions. Part of the chemisorbed F-ions penetrate into the Si forming a fluorosilyl layer. Via a number of subsequent processes SiF_4 is formed and desorbs from the surface. [21]

With high fluences and parallel incidence of the CO_2 irradiation, decomposition of SF_6 may occur due to coherent and multiphoton absorption (via the vibrational state ladder) resulting in its dissociation. [22] SF_6 molecules decompose into SF_5 and F atoms. SF_5 (being very unstable) decomposes into SF_4 and another F atom, which both diffuse into the Si surface and react to form SiF_4. Gas-phase photodissociation of SF_6 producing fluorine radicals has also been demonstrated for intense femtosecond irradiation at 800 nm. [20] Finally, Lowndes et al have suggested that fluoride compounds such as SiF_2 and SiF_4, which are volatile at the transient temperatures reached during laser heating, can be formed under irradiation of Si with a KrF (λ=248 nm, τ=25 ns) excimer laser. [21]

Figure 2.20 shows a possible scenario of how etching of the surface via photodissociation of SF_6 may take place. [23]

1. A silicon surface is exposed to femtosecond laser pulses in the atmosphere of SF_6.

2. Intense femtosecond laser pulses disrupt the molecules close to the surface, where the fluence is high (the laser light is focused onto the surface). This creates reactive fluorine radicals.

3. The radicals react with (possibly liquid) silicon and form SiF_x compounds.

4. SiF_x compounds are desorbed by the laser and then volatile species (such as SiF_4) leave the surface.

The aforementioned scenario explains the process of material removal via laser assisted chemical etching. Given the fact that bluntcones are produced in the absence of the gas, it is most likely, that the spikes are formed through a combination of both ablation and chemical etching of the surface. One possibility is that ablation produces structures that are sharpened by the gas.

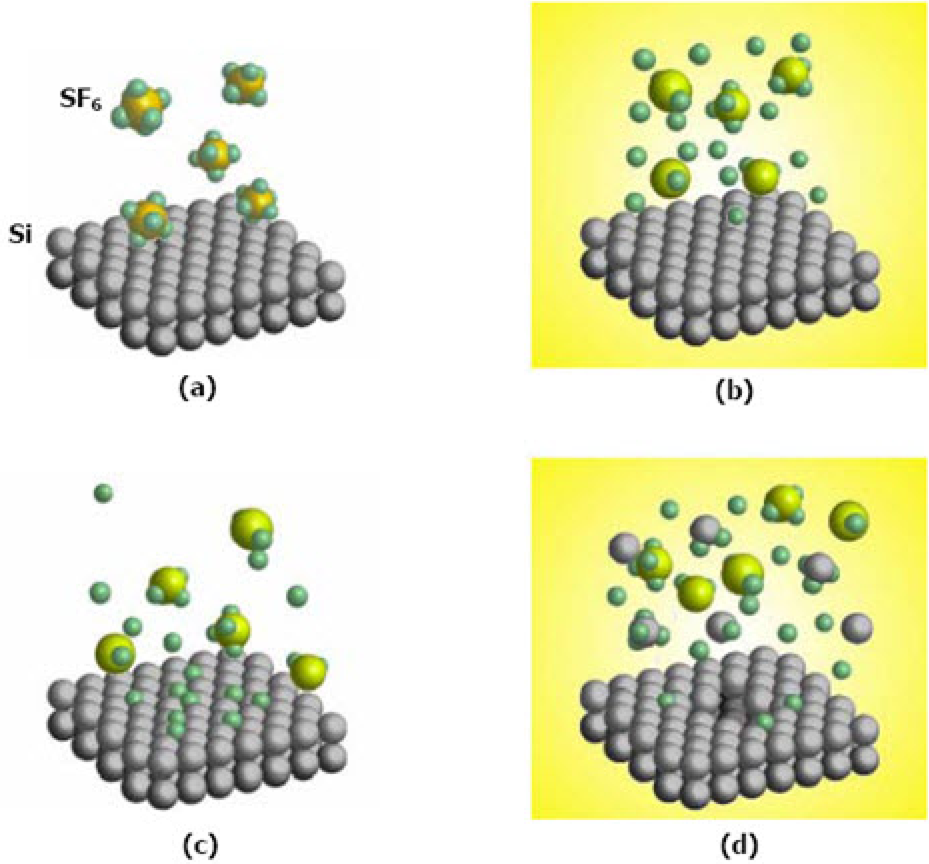

Figure 2.20: Possible interaction mechanisms of SF_6 with Si. [23]

2.3.3 Formation process of the nanometer-scale structures

Mazur et al have explained the formation process of the nanometer-scale ripples and rods in their work. [28] In this section, the proposed formation mechanisms are mentioned. The morphologies, observed upon laser irradiation in water environment, can be attributed to laser interaction with the silicon/ water system: ultrafast melting and resolidification at low fluence.
At low fluences (below the ablation threshold of silicon in water), the laser fluence is still intense enough to cause ultrafast melting. The spacing of the ripples is reduced to around 120nm. During the irradiation of silicon with a femtosecond pulse in the low-fluence regime, the front portion of the laser pulse excites a large number of electrons increasing the index of refraction in a thin surface layer of silicon. Within this high-index layer, the effective wavelength of refracted and scattered light is reduced, and the periodicity of the inter-

ference pattern is likewise reduced. Approximately one picosecond after the laser pulse strikes the surface, ultrafast melting produces a liquid layer whose evolution is dictated by surface-wave driven growth dynamics. The periodic absorption excites nanometer-scale surface waves in the liquid layer, and upon resolidification, nanometer-scale ripples are frozen into the surface.

The surface morphology after laser irradiation is due to the interplay between surface wave dynamics and the lifetime of the molten layer. Taking into account that the melt depth is large compared to 120 nm, the lifetime τ of a capillary wave is proportional to the square of its wavelength λ, $\tau = \lambda^2/8\pi 2\nu$, where ν is the kinematic viscosity of the liquid. Taking ν to be $2 \cdot 10^{-7} m^2/s$, we obtain a lifetime of approximately 1 ns for a capillary wave with a wavelength of 120 nm. For surfaces irradiated in a gas, the lifetime of the melt is longer than 30 ns, much longer than the lifetime of a surface wave with a wavelength of 120 nm. By the time the surface resolidifies, any nanometer-scale surface waves have died out and been replaced by surface waves with longer wavelengths and longer lifetimes. The thermal conductivity of water, however, is over 1 order of magnitude higher than that of a typical gas, and water vaporizes and dissociates on the substrate surface. The larger thermal conductivity of the water and the vaporization and dissociation of water result in a large heat transfer out of the molten layer, and so the lifetime of the molten layer in water is less than 1 nanosecond. The presence of water and the associated increase in the cooling rate of the molten layer allow for the nanometer-scale ripple patterns to be frozen into the surface before they die away.

During the second irradiation step nanometer-scale rods form along the straight nanometer-scale ripples. Although the second irradiation is at much lower fluence than the first one, the laser pulses melt the nanometer-scale ripples, because the absorptance of a rippled surface is higher than that of a smooth surface. Once they are molten, the ripples tend to break up into beads. As in the formation of the ripples, the scale of beads is set by the interference between incident and scattered laser light below the surface, which produces a periodic absorption pattern along the long axis of the ripples and excites a surface wave along the length of the ripples. Once the ripples break up into beads, subsequent laser irradiation sharpens the beads into rods through preferential removal of material around the beads by laser-assisted ablation.

Chapter 3

Optical Properties of Laser Structured Si

3.1 Introduction

Silicon (Si) is the most commonly used semiconductor in the field of optoelectronics as it can be easily integrated in electronic devices, detect visible light and function as a solar cell. However, silicon shows some drawbacks and its use is limited concerning specific applications. First of all, silicon is poorly used as light emitting diode because of its indirect band gap. Si cannot detect, also, important communication wavelengths and cannot exploit the whole sun's light spectrum, as silicon's light absorption decreases for wavelengths above 1.1μm due to its energy band gap (1.07eV). Consequently, ordinary crystalline Si cannot convert efficiently the energy of sunlight into electricity and, additionally, it is unsuitable for applications, such as telecommunications and scientific instrumentation which are based mainly on the absorption of the infrared region of light.

Great research efforts have been made in order to overcome these limitations. Use of different semiconducting materials or compounds (Ge, InGaAs, etc.), which can detect in the near infrared, is an alternate solution. However, near infrared detectors based on silicon technology could be produced in lower cost and facilitate integration with other microelectronics. Laser-assisted microstructuring of Si wafers (silicon spikes) is a novel approach of improving the optical properties of silicon. Upon laser processing, silicon surface obtains a velvet black color (black Si, Figure 3.1), providing a clear indication of the induced change in the optical properties with respect to the original, grey surface. This change can be, certainly, correlated with the absorption in the visible spectral range. Femtosecond laser structuring in the presence of

SF_6 ambient can enhance, greatly, the absorption of Si in near infrared as well.

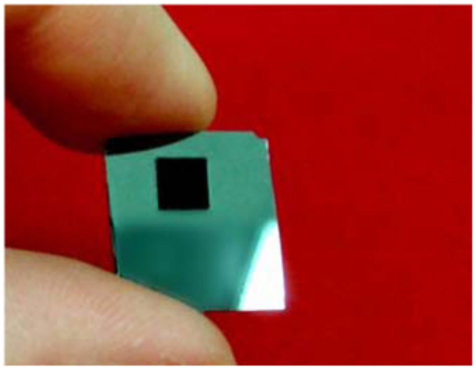

Figure 3.1: Top view of a femtosecond laser structured Si surface (black area) with respect to the flat Si surface (grey area)

In view of the infrared absorption of laser-textured silicon, it seems to be interesting to point out the optical behavior of ordinary silicon. In crystalline silicon, light can be absorbed when the energy of the incident photon is greater than silicon's band gap energy. The energy from the absorbed photon promotes an electron from the valence band to the conduction band, leaving a hole in the valence band. However, the minimum energy of the conduction band and the maximum energy of the valence band correspond to different k-vectors in k-space (indirect gap). Therefore the absorption of photons is indirect.

Indirect photon absorption means that the excitation of an electron from the valence to the conduction band at energies near the energy band gap requires simultaneously the change of electrons momentum by absorption or emission of a phonon. The indirect band gap lies at 1.07eV at room temperature. For energies exceeding the band gap energy, there is an abrupt absorption increase. In contrast, photons with energies less than the band gap energy cannot be absorbed by silicon, unless the photon flux is sufficiently great to produce multi-photon absorption. Taking into account the absorption of crystalline silicon, the observed infrared absorption in microstructured silicon is quite impressive.

The optical properties of laser structured Si have been studied from different research groups. Mazur et al. have investigated the advantages offered by femtosecond laser processing on the optical response of Si structured surfaces. [29, 30] Furthermore, Zorba et al. have implemented different laser sources with variable pulse durations in order to examine the influence of these laser parameters on the improvement of the optical behavior. [27]

In this study, we examine the optical properties of laser-patterned Si fabricated in constant gas ambient and in water environment. The irradiating source is constituted by a regenerative amplified Ti:Sapphire laser (λ=800nm) delivering 200fs pulses at a repetition rate of 1kHz. The fabricated Si samples consist of structures at the micrometer and nanometer length-scale. The absorptance of these Si structures is measured as a function of the wavelength.

3.2 Optical parameters

Three processes can take place when light impinges on a substrate: reflection, transmission, and absorption. Reflectance (R), Transmittance (T) and Absorptance (A) are related through the equation [31]:

$$R(\lambda) + T(\lambda) + A(\lambda) = 1 \tag{3.1}$$

In electromagnetism, the relative contribution of each process is determined by a material-dependent complex refractive index [32]:

$$\bar{n} = n + ik \tag{3.2}$$

The real part n is called the refractive index and relates the velocity of light in a medium to that in vacuum:

$$v_{medium} = \frac{c}{n} \tag{3.3}$$

where c is the velocity of light in vacuum.

The imaginary part k is called the extinction coefficient and is a measure of the absorption in the material. The absorption coefficient, α, of a medium is defined by the well-known Lambert-Beers Law: the transmittance, T=I_t/I_i , of a layer decreases exponentially with the distance traveled through the layer (z), where Ii is the incident intensity and It is the transmitted intensity. [32]

$$I_t(z) = I_i e^{-\alpha z} \tag{3.4}$$

with

$$\alpha = \frac{4\pi k}{\lambda} \tag{3.5}$$

where α^{-1} is the distance by which the incident flux has decreased to 1/e and is called penetration depth.

For normal incidence of light from air to the material, the reflectance of a material, defined as the reflected to incident intensity ratio, is expressed as [32]:

$$R \equiv \frac{I_y}{I_i} = \frac{(1-n)^2 + k^2}{(1+n)^2 + k^2} \tag{3.6}$$

3.3 Optical Measurements

3.3.1 Optical properties of micro-textured Si

The total hemispherical reflectance (R) and transmittance (T) of our Si samples are measured, directly, from the near ultraviolet (0.25μm) to the near-infrared (2.5μm) using a spectrophotometer, equipped with an integrating sphere. The use of the integrating sphere is necessary for the reflectance and transmittance measurements of a strongly scattering material. The absorptance (A) of the samples can be determined via the relation: A(λ)=1-R(λ)-T(λ).

Typical reflectance, transmittance and absorptance spectra of the microstructured Si substrates are shown in Figure 3.2. The corresponding spectra of unstructured Si surfaces are also shown. The drop in the absorptance for crystalline silicon near 1100nm corresponds to the band gap energy of crystalline silicon (1.07eV). Light at longer wavelengths does not contain enough energy to promote an electron from the valence band to the conduction band and absorption becomes negligible for crystalline silicon.

On the other hand, microstructured silicon has a drastically decreased reflectance and transmittance over the entire measured spectrum. The lowered transmittance and reflectance result in near-unity absorptance in the entire wavelength region 250 nm$<\lambda<$ 2500 nm. The increased absorption in the visible is consistent with the black appearance.

In particular, crystalline silicon is highly reflective across the electromagnetic spectrum due to its high refraction index. Therefore, a substantial amount of light is not absorbed. The absorption for this type of silicon changes abruptly and decreases to essentially zero for below-band gap energies. Therefore, only energy greater than the band-gap energy can be absorbed.

Below band gap absorption in crystalline Si is feasible by introducing impurity atoms or changing the structural order of the crystal lattice. In the first case, the introduction of impurity atoms, which means the replacement of Si atoms with donor or acceptor atoms in the lattice, involves the introduction of energy states in the forbidden band gap. This occurs due to the

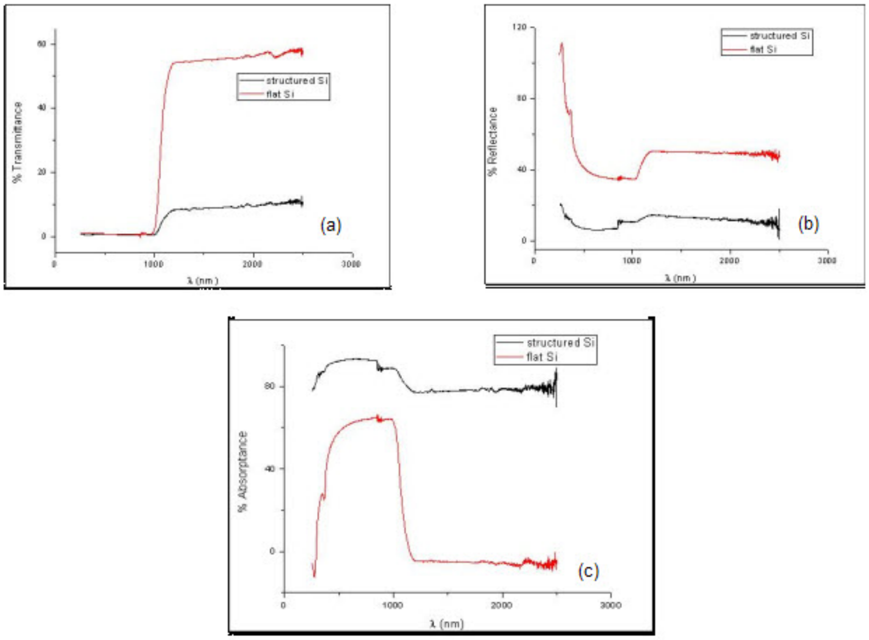

Figure 3.2: (a) Transmittance, (b) Reflectance, and (c) the calculated Absorptance of Si laser-structured. The same measurements are shown for unstructured, single crystalline Si for comparison

fact that the impurity atoms bind the electrons with a different potential. In contrast, structural changes cause modifications in the periodic crystal lattice and, thus, lead to the introduction of energy levels in the band gap. The existence of these states within the band gap allows the absorption of photons with below-band gap energies. Transitions from or to these states can take place during the interaction of light irradiation with Si samples. The below-band gap absorptance occurs in amorphous or polycrystalline silicon. However, the production of band tails of localized states within the gap is inevitable due to structural disorder. [34**?** , 35]

The spectra shown in Figure 3.2 reveals light absorption at below-band gap wavelengths (>1.1μm), where crystalline silicon does not normally absorb, indicating that modifications on silicon's microstructured surface could be responsible for the improved optical response. In the following section, we examine the effect of laser fluence on Si optical properties.

The effect of laser fluence

In this section, the effect of laser fluence on the optical response of the laser-processed silicon structures fabricated under 500 Torr of SF_6 is studied.

In particular, we measure the reflectance and transmittance and determine the absorptance for flat and micro-patterned substrates with different surface morphologies. All samples are made from Ph-doped Si (100) wafers.

The calculated absorptances for two micro-textured surfaces and a flat, unpatterned surface are depicted in Figure 3.3. The increased absortance of the laser-processed Si substrates is accompanied with a remarkably decreased reflectance and transmittance over the entire measured wavelength region. The lowered transmittance and reflectance lead to a near-unity light absorptance even for energies which correspond to the infrared region of light spectrum.

For structured silicon, the reflectance and the transmittance are less than that for flat silicon. For the samples fabricated in a 500 Torr of SF_6 atmosphere, increased absorptance (>90%) is observed for all above-band gap wavelengths. The absorptance for the below-band gap wavelengths increases with increasing laser fluence. The value of the below-band gap absorptance remains constant in the wavelength range (∼1300-2500nm). Consequently, the absorptance is greater for the patterned surfaces, and in particular, the taller the structures are, the greater the absorptance is.

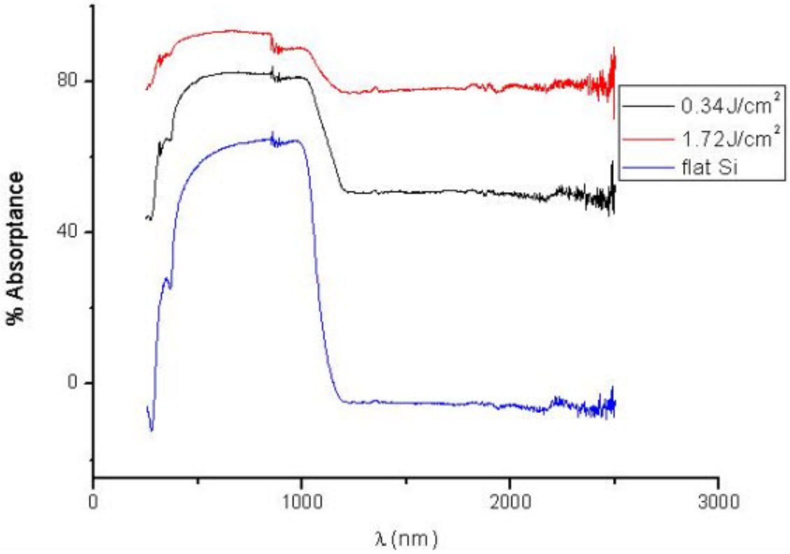

Figure 3.3: Absorptance of laser-fabricated Si microstructures as a function of the wavelength for different fluences

3.3.2 Optical properties of nano-textured Si

The optical properties of crystalline Si are influenced upon laser processing in water. In the wavelength range between 350nm and 1000nm, the absorptance of silicon ripples is about 90%, while the absorptance of the nanorods is about 95% (Figure 3.4). Upon laser nano-processing, silicon surface obtains a velvet black color, providing a clear indication of the induced change in the optical properties with respect to the original, grey surface. This change is, certainly, correlated with the increased absorption in the visible spectral range. The drop in the absorptance for crystalline silicon near 1100nm corresponds to the band gap energy of crystalline silicon (1.07eV). This drop appears, also, in the case of the nano-structured Si. Furthermore, increase in the absorptance of the infra-red light is not observed.

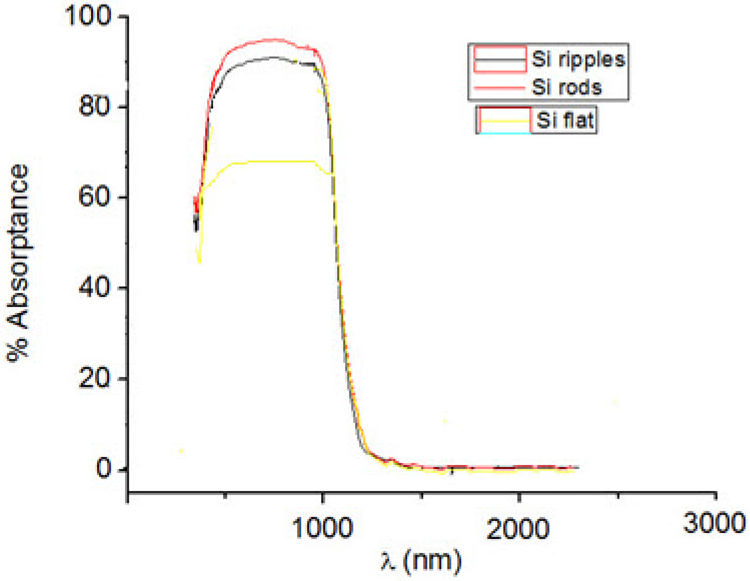

Figure 3.4: Absorptance of laser-fabricated Si nanostructures as a function of the wavelength for different fluences

3.4 Discussion

There is an increased absorptance, close to 95%, observed in the visible spectral range. The enhancement in light absorption of micro- and nano-structured Si substrates can be attributed to the reflection reduction. [30] The Si structures are on larger scale than the wavelength of the incident irradiation, therefore, multiple reflections among the structures can take place and the light irradiation, as a result, is trapped. This can cause increase in light absorption. This indicates that Si structures can enhance the absorptance of visible light.

However, the induced increase in absorptance cannot depend, only, in multiple reflections concerning the micro-sized spikes. Reduced reflection in the infrared would lead to increased transmittance in the infrared and not to increased absorptance. Structural and/or chemical modifications in Si samples may be responsible for the change in optical response in the infrared region of light spectrum. [30]

Chemical changes are strongly related with the presence of foreign atoms in the crystal lattice, which create absorbing states in the forbidden band gap. The silicon wafers that we use for laser processing is n-doped, with phosphorous (group V) being the dopant. In general, highly-doped silicon can absorb infrared irradiation. Although our wafers are doped, the concentration of the impurities is not sufficient enough in order to induce such dramatic changes in the infrared light absorption. This can be seen from the absorption spectrum of the flat, unpatterned silicon. It is obvious, that the absorptance is close to zero at the infrared region. However, structuring n-doped Si wafers can cause diffusion and redistribution of dopants that could have formed an infrared absorbing layer. Though, the silicon microstructures are heavily sulfur-doped. During the laser-assisted silicon processing, impurities from the ambient environment are incorporated into the structures. The sulfur atoms are, thus, strong candidates for forming the infrared absorbing layer and introducing energy levels (donor levels) in silicon's band gap. [30] The high concentration of sulfur embedded in the spikes (on the order of $10^{20}/cm^3$) is expected to form an energy band in the band gap. Then the absorption of photons with energies below the band gap of ordinary Si is enabled, making it possible for infrared light to promote electrons from these impurity states into the conduction band.

3.5 Applications

The high absorptance of micro-structured silicon in the visible and especially in the infrared spectral range could have potentially important technological applications. In photovoltaics technology, solar cells and photodetectors are made, mainly, from silicon. Since silicon presents high reflectance across the electromagnetic spectrum, additional treatments are necessary in order to reduce the reflection of the silicon surface. Fabricating micro-structures on a crystalline silicon surface is an efficient method to reduce light reflection, since the laser-structured surface exhibits near-zero reflection over a broad wavelength range ($\sim$ 250-2500nm). If the increased light absorption leads to the production of photocarriers, silicon spikes could be used to improve the quantum efficiency of the existing photovoltaics.

Additionally, the near-unity light absorption of below-band gap radiation could attract scientific interest. Infrared detection is of great importance to many fields, such as telecommunications, remote sensing or space research. If the absorptance of below-band gap radiation creates photocarriers for conduction, spiked silicon could fundamentally change infrared detection technology.

Chapter 4

Wetting Properties of Laser Structured Si

4.1 Introduction

Laser microstructuring of materials surfaces has attracted a lot of scientific interest in a wide range of applications, such as micro-fluidics, biological scaffolds, self-cleaning surfaces and lab-on-chip devices. [36, 37, 48] This increasing interest is attributed to the possibility of controlling the wetting properties of the micro-engineered surfaces, and specifically inducing superhydrophilic and superhydrophobic behavior. Superhydrophobic surfaces are provided by nature. In particular, the lotus leaf exhibits water-repellent behavior, which is ascribed to its complex morphology present on its surface, comprising hierarchical structuring at both the micrometer and nanometer length-scale. [49] Due to its unique wetting properties, lotus leaf surface is considered as a model superhydrophobic surface. Mimicking surface morphologies, which exist, in abundance, in nature, has proven to be an efficient way of fabricating artificial superhydrophobic surfaces. Therefore, simplified techniques of manufacturing such complex surface topologies, providing reproducibility, are expedient.

Photolithography, templated electrochemical deposition, plasma treatments and electron-beam lithography are different patterning approaches for fabricating surfaces, in order to control their wetting properties. [40–43] However, simple one-step production techniques, without the need of clean-room facilities and high-vacuum equipment requirements, are more attractive. Laser micro-structuring of solid materials in specific ambient environments concentrates the desired features. The produced Si surfaces consist of forests of conical spikes exhibiting controlled dual-scale roughness at the micrometer and nanometer scale. Silicon spikes obtain a characteristic size from a few to tens of μm, decorated by protrusions in the scale of tens to a few hundreds of nm on their walls. [44] This laser-based technique is applicable in a wide range of materials, such as ceramics, polymers, or metals so as to tailor their surface morphology, and thus control materials surface wettability. [45–47]

Different research groups have studied, thoroughly, the wetting properties of the laser structured Si surfaces coated, also, by various conformal layers. Mazur et al. have studied the wetting properties of laser structured Si coated by fluoroalkylsilane molecules. [48]. Zorba et al. have managed to tune the wetting response of Si, from initially hydrophilic to hydrophobic, through femtosecond laser structuring, without any surface coating. [44] Spontaneous motion of liquids was induced; it was possible to drive drops to ascend a structured Si surface, tilted at any angle by fabricating a proper texture gradient on it.

In the present work, we study the wetting response of Si surfaces structured in a 500 Torr of SF_6 atmosphere and in water environment, using the Ti:Sapphire femtosecond laser source (λ=800nm, τ=200fs). In particular:

• Using femtosecond laser structuring we are able to fabricate Si based surfaces exhibiting double-length scale roughness. Variable roughness at the micrometer scale can be achieved by changing the laser pulse fluence in the presence of a reactive gas and control over the wetting properties of Si is obtained. Change in Si wettability is achieved upon laser processing in water. The behavior of structured Si substrates can switch from hydrophilic to hydrophobic without any additional surface coating. Static contact angle measurements are performed by an automated tensiometer, using the sessile drop method, in order to assess the wetting response of Si.

4.2 Fundamentals

4.2.1 Young's Equation

A small liquid droplet deposited on a solid surface either forms a spherical cap with a well-defined equilibrium contact angle θ to the solid or it spreads across the surface, forming a wetting film (Figure 4.1). The balance between the surface tensions (γ) at the three-phase contact line formed along the solid-liquid, liquid-gas and solid-gas interfaces determines the shape of the drop. The force balance leads to the Young equation:

$$\gamma_{lg} cos\theta_o = \gamma_{sg} - \gamma_{sl} \tag{4.1}$$

where the subscripts (sg), (sl), and (lg) correspond to solid-gas, solid-liquid, and liquid-gas interfaces respectively. Young contact angle (θ_o) is the angle at which a liquid-gas interface meets the solid surface and for this, the energy of the system reaches a local minimum. [49–51]

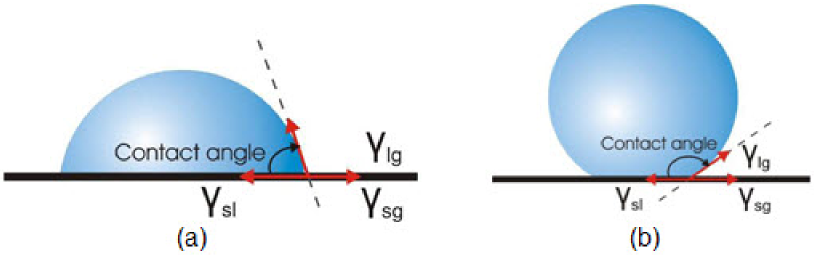

Figure 4.1: A sessile liquid drop on (a) a hydrophilic and (b) a hydrophobic surface

Depending on the value of the contact angle, a surface can be characterized as hydrophilic (<90^o) [Figure 4.1 (a)] or hydrophobic (>90^o) [Figure 4.1 (b)]. The contact angle is, thus, a measure of the wetting behavior of a given surface.

Surface tension is a balance of the intermolecular forces at a surface and is defined as the energy (W) needed to increase the surface area per increase in surface area (A):

$$\gamma = \frac{dW}{dA} \tag{4.2}$$

High interfacial surface energy for the liquid-solid results in a large contact angle, i.e. the higher the surface tension of the liquid, or the lower the surface energy of the substrate, the larger the contact angle. With water, typically the most hydrophobic flat solids can reach up to $\theta \sim 120^o$. An even more hydrophobic surface can be obtained by structuring, which will enhance the overall roughness and, thus, change the wetting behavior of the surface.

4.2.2 Wettability and surface roughness: Wenzel and Cassie Baxter states

The surface roughness affects the wetting response of the surfaces. Two different models, the Wenzel model and the Cassie Baxter model respectively, approach in a theoretic level the effect of the induced surface roughness on the wetting behavior of the structured surfaces.

In the Wenzel model, it is considered that the liquid completely penetrates the entire rough surface, without leaving any air pockets underneath it

(Figure 4.2 (a)). [52] The contact angle θ_w, is given by the following equation:

$$cos\theta_w = rcos\theta_o \tag{4.3}$$

where r is the ratio of the unfolded surface to the apparent area of contact angle under the droplet, and θ_o is the contact angle on a flat surface of the same nature as the rough (Young contact angle). Since r is always greater than unity, this model predicts that the contact angle will decrease/ increase with surface roughness for an initially hydrophilic (θ<90^o)/ hydrophobic (θ>90^o) surface.

In contrast, in the Cassie and Baxter model it is assumed that the liquid does not completely permeate the rough surface because air gets trapped underneath it. [53] As a consequence, the liquid droplet will form a composite solid-liquid/ air-liquid interface with the sample in contact, and the effective surface energy of the scaffold below the water will be dominated by air. In this case, the apparent contact angle θ_{CB}, is an average of the flat surface, θ_o, and the value for full hover over the flat surface (that is 180^o) and is given by:

$$cos\theta_{CB} = -1 + f + r_f f cos\theta_o \tag{4.4}$$

In the above expression, θ_{CB} is the Cassie-Baxter contact angle (equation 4.4), f is the fraction of the projected solid surface that is wet by the liquid, andr_f is the roughness ratio of the wet area. [53, 54]

When the liquid drop is lying on the top of the rough surface without sinking into the features at all (Figure 4.2 (b)), the roughness factor will equal one (r_f=1) and equation 4.4 becomes the widely used simplified form of the Cassie-Baxter equation.

$$cos\theta_{CB} = -1 + f(1 + cos\theta_o) \tag{4.5}$$

As f is always lower than unity, this model always predicts enhancement of the hydrophobicity, independently of the value of the initial contact angle θ_o. The lower the value of f, the higher the contact angle measured.

In contrast, when f=1 and r_f=r, equation 4.4 turns into the Wenzel equation.

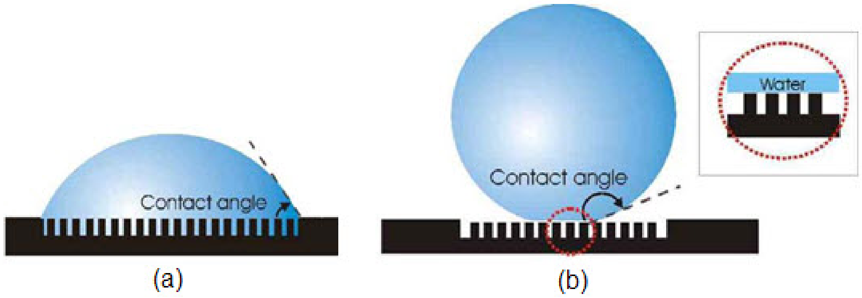

Figure 4.2: A liquid drop (a) in the Wenzel state and (b) in the Cassie-Baxter state

4.3 Hydrophobic laser-structured Si surfaces

4.3.1 Wetting properties of micro-textured Si

An initially hydrophilic Si surface can become hydrophobic through femtosecond laser microstructuring of Si wafers in a reactive gas atmosphere. Structuring of Si results in the enhancement of its overall surface roughness. Measurements of the static contact angles of 3μl distilled, deionized Millipore water (18.2 MΩ) drops deposited on a flat and a structured Si surface can show the difference in the wetting behavior of Si surface in combination with the change of surface roughness. An automated tensiometer is used to determine the contact angle and is based on a collection of images of sessile drops. The drop is formed from a capillary tip, and is gently detached from the tip onto the silicon substrates.

Figure 4.3 (a) and (b) depict the contact angles of a water drop on an unstructured Si surface and on a laser textured Si surface, respectively. In the first case, the value of the contact angle can achieve up to $\theta{\sim}65^o$, whereas, in the case of the structured Si the value comes up to $\theta{>}140^o$.

The structured Si samples were fabricated using the Ti:Sapphire laser source in the presence of reactive SF_6. Prior to the contact angle measurements, all the samples were immersed in a 10% HF aqueous solution, in order to remove the oxide layer grown on the surface during the laser irradiation process.

Morphology and static contact angle measurements

In this session, we investigate the wetting response of microstructured Si samples in correlation with the different morphologies applied on them. Silicon microstructures have been fabricated with superior control of structure

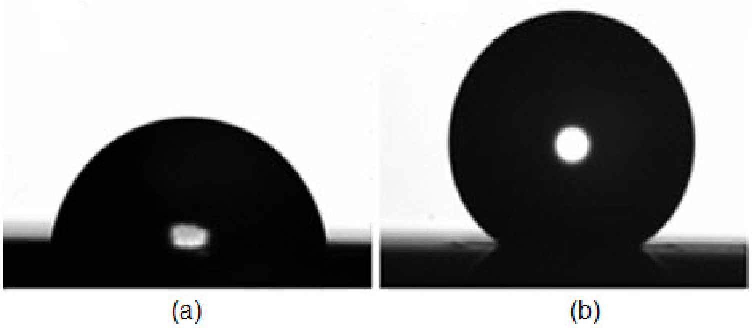

Figure 4.3: Static contact angles of a 3μl nanopure water drop deposited on (a) an unstructured Si surface and (b) a femtosecond laser microstructured Si surface

geometry and pattern regularity through ultrafast laser processing. Each processed Si surface is fabricated at different laser fluences and the patterned areas comprise forests of conical microstructures (spikes) exhibiting structures at the micro- and the nano- scale. As we have mentioned, variations of laser fluence cause remarkable changes in the structures as to shape, dimension and density. By increasing laser fluence, conical microstructuring is promoted on the Si surface, with structures becoming more pronounced and spatially separated.

Besides directly affecting the micrometer-scale surface topology, increasing fluence is also crucial to induce a more pronounced sub-micrometer decoration on the spikes' walls. The spikes' height varies from one to ten micrometers, while the size of nano-protrusions ranges from tens to a few hundreds of nanometers, providing a double length-scale pattern on the silicon surface. The second length-scale pattern on the Si surface becomes more evident as the laser fluence increases. The micrometer-scale features, together with the nano-scale protrusions result into a significant increase of the overall roughness. Pictures of the water droplets lying on the structured Si surfaces are shown in Figure 4.4.

From Figure 4.4, we see that the contact angle of the microstructured substrates increases with increasing laser fluence. This means that the wetting properties of the patterned Si samples depend greatly on the structures topology. The laser fluence dependence of silicon's wettability is depicted in Figure 4.5. The initial hydrophilic surface is converetd to a hydrophobic one upon femtosecond laser microstructuring.

It is obvious that the laser-based Si structuring modifies the overall surface morphology and roughness and, therefore, the wetting response of Si changes. The wetting behavior of the structured Si follows the Cassie-Baxter model

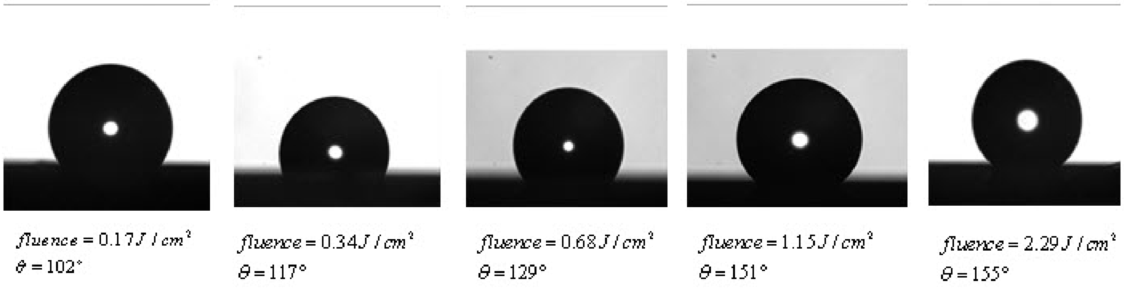

$fluence = 0.17 J/cm^2$
$\theta = 102°$

$fluence = 0.34 J/cm^2$
$\theta = 117°$

$fluence = 0.68 J/cm^2$
$\theta = 129°$

$fluence = 1.15 J/cm^2$
$\theta = 151°$

$fluence = 2.29 J/cm^2$
$\theta = 155°$

Figure 4.4: Static contact angles of a 2μl nanopure water drop deposited on fs laser structured Si surface

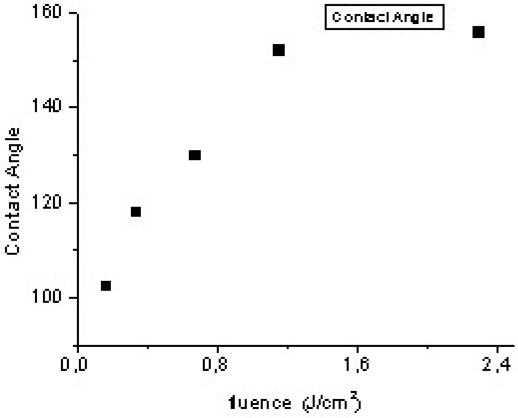

Figure 4.5: Laser fluence dependence of microstructured Si contact angles

which predicts enhancement of hydrophobicity with increasing surface roughness ratio.

4.3.2 Wetting properties of nano-textured Si

In this subsection, we examine the wetting response of nanostructured Si substrates formed by laser structuring in water environment. As we have mentioned, straight ripples and high density arrays of rods at nanometer-length scale are formed on Si surface upon laser irradiation at low fluence regime. In order to assess the wetability of the nano-patterned samples, contact angle measurements are perfomed. Pictures of the water droplets lying on the structured Si surfaces are shown in Figure 4.6

We observe that there is an increase in contact angle of Si upon laser nanos-

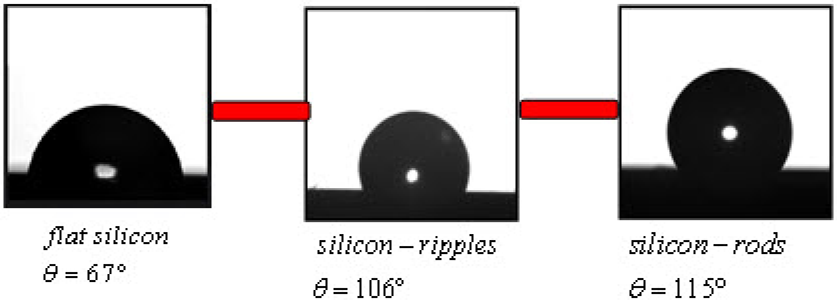

Figure 4.6: Static contact angles of a 3μl nanopure water drop deposited on (a) flat Si, (b) nano-rippled and (c) Si covered with nano-rods

tructuring. This means that the wetting behavior of Si depend on its surface morphology. Furthermore, there is an enhancement of Si hydrophobicity with increasing roughness ratio, which is consistent with the Cassie-Baxter model.

4.4 Discussion

Among the advantages of using laser processing for the formation of self-organized surface features, is that it can be applied in a wide range of materials, such as polymers, ceramics, or metals in order to control surface topology, and thus open the way to controlling their wettability. Furthermore the possibility of using these Si surfaces as masters for replication of the surface morphology on different materials as has been shown in other studies, makes possible for the combination of laser based techniques and standard replication processes to lead to the manipulation of the wetting response of materials. [27] Materials with tailored wetting response can find use in self cleaning, microfluidics, lab-on-chip devices, chemical sensors, water-proof surfaces etc.

More specifically, in this chapter we have demonstrated the use of laser structuring for tailoring the wetting response of Si surfaces. In particular we have found that fs-laser irradiation may be employed to render Si hydrophobic without any additional surface coating. The resulting structures consist of double-lengthscale roughness, and we achieved an enhancement of the water contact angle from 67^o to greater than 150^o.

Chapter 5

Biological Applications of Laser Structured Si

5.1 Introduction

Laser-structured micro and nano rough Si scaffolds with controllability of roughness ratio and surface chemistry can serve as a novel means to elucidate the 3D cell-biomaterials interactions in vivo. In this chapter, it is demonstrated that the wettability of such artificial substrates can be preferentially tuned from super-hydrophobic to super-hydrophilic through independently controlling roughness ratio and surface chemistry. The dependency of fibroblast cell response on the artificial structures is systematically investigated and clarified that a fundamental parameter that determines cell adhesion on 3D substrates is not solely the degree of roughness or surface chemistry but the synergy of both, which determines the wettability or surface energy of the culture substrate.

As it was mentioned, the ability of biomaterial surfaces to regulate cell behavior requires control over surface chemistry and microstructure. One of the greatest targets with silicon-based biomaterials is to improve biocompatibility and tissue integration. This may be achieved by modifying the exposed silicon surface with bioactive peptides (Arg-Gly-Asp) The effect of such biofunctionalized surfaces on fibroblast cell adhesion ad proliferation should be investigated. In this work, we examine the covalent attachment of amyloid peptides on the laser-structured Si substrates. A further step should be the conjugation of bioactive peptides on the silicon microstructures.

5.2 Fibroblast cell response of laser-structured Si

5.2.1 Introduction

The main target of artificial cell culture scaffold design is to mimic the natural extracellular environment features, in a way that cells can function as if they in vivo. In this respect, designing surfaces for controlling cell-material interactions is a considerably interesting subject, highly significant in the development and eventual success of implantable medical devices and engineered tissues. [74–76] Using different approaches, various materials have been surface engineered in order to guide cell adhesion and modulate cell-biomaterial interactions [77–79], indicating that cell growth, division and migration are highly dependent on their immediate culture substrate. Hence, surface chemistry [80, 81], wettability [82, 83] and roughness [75, 84] are found to be three of the most important factors influencing biological reactions at biomaterial surfaces. [85]

There is, however, increasing evidence indicating that cell-surface interactions occur at multiple length scales. [79] Indeed, in the context of a natural environment, the cells included in a tissue are surrounded by a three-dimensional (3D) dynamic extracellular matrix (ECM), which provides instructive cues at meso- micro- and nanoscales necessary to maintain cell phenotype and behavior. Therefore, in order to reach the level of ECM complexity, biomedical substrates must interlace hierarchically organized multiple-scale structures. Due to such demanding design requirements, cell response on sub-micrometer as well as micrometer scale rough substrates, has not yet been systematically studied. Thus, the production of surface engineering schemes enabling controlled and reproducible structuring of biomaterials at both micro- and nano- scales, is required. [86]

Furthermore it should be outlined that cells are inherently sensitive to variations of surface chemistry. [79] Consequently,there is the question of whether cell behavior, related to viability, proliferation, motility, adhesion, morphology, cytoskeletal arrangement and gene expression, is influenced by the topographical features and/or the surface chemistry of a scaffold, parameters that determine the surface tension and wettability. [87] In order to overcome such controversies, it is crucial to find pathways to discriminate among the different effects. In this respect, the ability (a) to control the surface chemistry, while keeping the same micro/nano morphology or vice versa and (b) to tune surface wettability from super-hydrophobicity to super-hydrophilicity are highly important tools allowing successful attachment of fully functional cells to biomedical surfaces.

The results of this work demonstrate the ability to tune cell adhesion using biomimetic artificial substrates in a 3D-design, comprising hierarchical micro- and nanostructures produced by ultrafast laser patterning of silicon (Si). Tailoring of the structures morphological features can be advantageously achieved by varying certain fabrication parameters. This capability allows one to control the wetting properties and thus, surface tension of the Si substrates. Further control over wettability can be achieved by altering the surface chemistry through coating the structures with various conformal layers, while keeping the same morphology. As a consequence, it is possible to preferentially tune the wettability of the artificial substrates from super-hydrophobicity to super-hydrophilicity through a proper combination of surface topography and chemistry.

Conclusively, it is demonstrated that the patterned Si substrates can be potentially used as model scaffolds for the systematic exploration of the role of 3D micro/nano morphology and/ or surface energy on cell adhesion and growth. The different structures obtained by this method can be transferred to various types of polymeric materials as well through replication molding techniques. [88] The simplicity of the structuring process and the flexibility of fast patterning by laser beam scanning, together with its potential to tailor the wettability of different classes of materials, are certainly useful for creating patterned interfaces on biomaterials devices.

5.2.2 Materials and methods

Micro and nanostructure fabrication

The fabrication of the silicon micro/nanostructures is based on ultrafast laser structuring as described in the second chapter. The structured Si surfaces comprise forests of conical spikes exhibiting controlled dual-scale roughness at both the micro- and the nano- scale. Variable roughness could be achieved by changing the laser pulse fluence.

In order to alter the surface chemistry, freshly prepared patterned surfaces are covered with either a thermally grown, hydrophilic oxide layer or with a hydrophobic silane coating through vapor adsorption from solution. Both layers are known to form high quality conformal coatings on Si surfaces. For oxidation, the samples are placed in a box furnace and heated at 1000 °C for 30min in air. For silanization, the samples are placed in a flask containing 0.5ml of dichlorodimethylsilane (DMDCS) reagent, where hydrophobic DMDCS monolayers are deposited on their surface via adsorption reactions. The silanization process employed is similar to that reported in the literature. [89].

Cell cultures

Prior to cell culture the structured surfaces are sterilized and then transferred onto sterile 6 well plates (Sarstedt; Numbrecht, Germany).

The NIH/3T3 cells are suspended to a concentration of 10^5 cells/ml in Dulbecco's modified Eagle's medium (DMEM) supplemented with 10% fetal bovine serum (FBS), and 1% antibiotic solution (GIBCO, Invitrogen, Kalsruhe, Germany) and 3ml of cell suspension is added in the 6 well plate and cultured at 37 °C , for 72h in an atmosphere of 5% CO_2. Before seeding the cells on the different surfaces, cells are grown to confluency, detached with 0.05% trypsin/EDTA (GIBCO, Invitrogen, Kalsruhe, Germany) and diluted in complete medium at an appropriate density. All experiments are done in triplicates to ensure reproducibility and obtain better statistics.

Cell viability assay

In order to assess cell viability, the Live-Dead Cell Staining Kit (BioVision) is used. The kit utilizes Live-Dye, a cell-permeable green fluorescent dye (Ex/Em = 488/518 nm), to stain live cells. Dead cells can be easily stained by propidium iodide (PI), a cell non-permeable red fluorescent dye (Ex/Em = 488/615). At the end of the incubation time (72h), structured surfaces with the cells are covered with the staining solution and incubated for 15min at 37 °C . Cells are observed immediately under a fluorescence microscope. Stained live and dead cells can be visualized by fluorescence microscopy using a band-pass filter (detects FITC and rhodamine). Healthy cells stain only with the cell-permeable Live- Dye, fluorescing green. Dead cells can stain with both the cell-permeable Live-Dye and the cell non-permeable PI (red), the overlay of green and red appears to be yellow-red. The experiments are done in triplicates and for each surface the mean number of live cells is calculated.

Laser scanning confocal microscopy

For the double staining of F-actin and Vinculin the focal adhesion staining kit (Chemicon International Inc., Temecula, CA, USA) is used. The cells are fixed with 4% paraformaldehyde for 15min and permeabilized with 0.1% Triton X-100 (Merck KGaA, Darmstadt,Germany) in PBS for 3-5min on ice. The non-specific binding sites are blocked with 1% BSA in PBS for 30min.

Actin and focal adhesion complexes are stained by incubating cells in diluted primary antibody (anti-vinculin) in blocking solution (1:200) for 1h and subsequently labelling them with diluted secondary antibody (1:200) (mouse-anti-mouse FITC conjugate) (Sigma- Aldrich Chemie GmbH, Munich, Germany) for 45min, with simultaneous incubation with diluted tetramethyl rhodamine isothiocyanate- conjugated phalloidin. The samples are then washed with PBS and stored in 10% glycerol in PBS in dark. Confocal microscopy is performed using a Zeiss AxiosKop 2 plus' laser scanning confocal microscope.

Scanning electron microscopy

The morphologies of NIH/3T3 fibroblasts seeded on patterned surfaces or on flat silicon wafer are observed by SEM. After incubation, cells are washed with 0.1M of sodium cacodylate buffer (SCB) and then incubated with the SCB for 15min. This step is repeated twice and followed by the fixation of the cells using a fixative buffer (2% glutaraldehyde, 2% formaldehyde in 1% SCB) for 1h at 4 °C . Subsequently, the surfaces are washed twice (from 15min each time) with 1% SCB at 4 °C . After that, cells are dehydrated through a graded ethanol series (from 10% to 100%) and incubated for 15min on dry 100% ethanol. Prior to electron microscopy examination the samples are sputter coated with a 10nm gold layer. SEM is performed on a JEOL 7000 field emission scanning electron microscope with an acceleration voltage of 10 kV.

Statistical analysis

Student's t-test is used to compare the significance levels ($p < 0.001$) between control and test values.

5.2.3 Results

Surface topography and wettability

The manufactured substrates, which possess a 3D-design, are produced by simultaneous structuring at both micrometer and nanometer length scales. As shown in the SEM micrographs of patterned Si surfaces produced at different incident laser energies per unit area (fluences, Figure 5.1(a) and (b)), the treated areas comprise forests of conical microstructures (spikes) exhibiting structures at the micro- and nano- scale. Variation of laser fluence caused remarkable changes in the structures as to ratio, dimension and density. Besides directly affecting the micrometer-scale surface topology, increasing fluence is also crucial to induce a more pronounced sub-micrometer decoration on the spikes' walls. In particular, the spikes' height varied from one to ten micrometers, while the size of nano-protrusions ranged from tens to a few hundreds of nanometers, providing a double length-scale pattern on the silicon surface (Figure 5.1 (b)). The micrometer-scale features, together with the nanoscale protrusions result into a significant increase of the overall roughness. Consequently, these etched substrates should allow more 3D free space perpendicular to the culture plane and should also provide physical cues to facilitate cell adhesion and spreading.

In this study, three series of substrates are tested: Type A corresponds

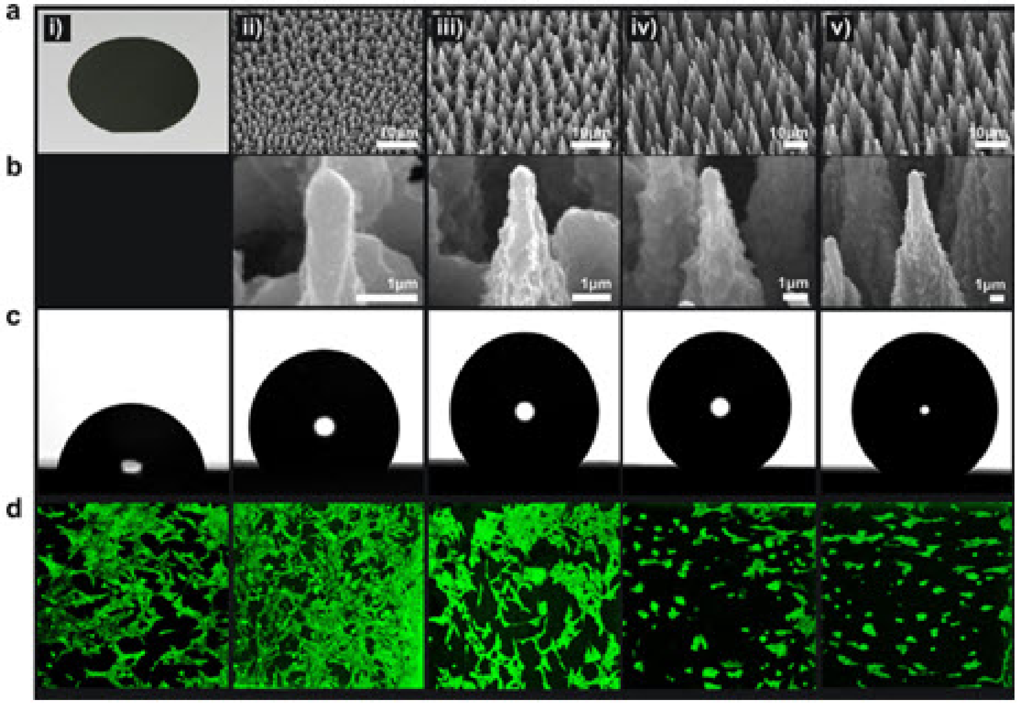

Figure 5.1: (a) Picture of a polished Si wafer (i) and side SEM views of the as-prepared Si spikes surfaces structured at four different laser fluences (ii) 0.34 J/cm^2 (A1), (iii) 0.56 J/ cm^2 (A2), (iv) 0.90 J/cm^2 (A3), and (v) 1.69 Jcm^2 (A4); (b) high magnification SEM images of the corresponding Si cones obtained; (c) photographs of water droplets on the patterned Si surfaces; and (d) confocal laser microscopy pictures of fibroblast cells cultured for three days on the respective surfaces.

to the, as-prepared, patterned Si surfaces comprising four samples with gradient roughness ratios, denoted as A1-A4; Type B corresponds to the same substrates coated with a hydrophilic thermally grown oxide layer (B1-B4); (c) Type C corresponds to the same substrates coated by a hydrophobic silane layer. Types A and C samples show the same qualitative results and will be considered as equivalent cases thereafter. In all series, the corresponding flat surfaces are tested as control samples. The principal properties of the above substrate types are summarized in Figure 5.2.

Images of water droplets lying on flat and as-prepared micro-structured Si surfaces are shown in Figure 5.1 (c). The corresponding dependence of the wetting angle (WA) on the laser fluence and roughness ratio attained is plotted in Figure 5.3 (a). It is evident that the laser-assisted texturing of Si induces a remarkable increase in its hydrophobicity which is more pronounced at high fluences.

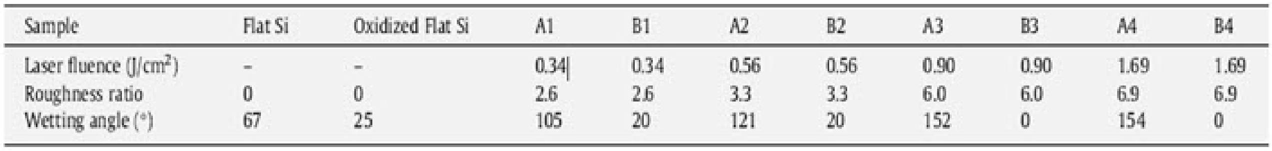

Sample	Flat Si	Oxidized Flat Si	A1	B1	A2	B2	A3	B3	A4	B4
Laser fluence (J/cm^2)	-	-	0.34	0.34	0.56	0.56	0.90	0.90	1.69	1.69
Roughness ratio	0	0	2.6	2.6	3.3	3.3	6.0	6.0	6.9	6.9
Wetting angle (°)	67	25	105	20	121	20	152	0	154	0

Figure 5.2: General properties of the different samples used for this study. Series A denote as-prepared patterned Si surfaces and series B denote the patterned surfaces after thermal oxidation treatment.

Cell spreading and viability

In order to investigate whether these surfaces are able to modulate cellular responses, cell adhesion experiments are performed using the fibroblast NIH/3T3 cell line. Optical and SEM photomicrographs of NIH/3T3 fibroblasts, seeded on patterned surfaces, show that both the cell concentration and shape are different depending on the culture substrate (Figure 5.1 (d) and Figure 5.4, respectively). The number of attached cells per unit area decreases as the roughness ratio and WA increase, denoting that cell attachment is favored on more hydrophilic surfaces. Concurrently, cell morphology changes from a well spread polygonal phenotype on smoother surfaces to a round-shaped phenotype on highly rough super-hydrophobic substrates and a smaller cell size, indicative of poor adhesion. Additionally, the SEM micrographs of Figure 5.4 show that in super-hydrophobic substrates, cells appear to accumulate and form multi-layers, probably due to limited opportunity for sufficient traction and stretch out in order to minimize unfavorable contacts with the substrate. This layer of elongated cells could serve as a basal structure for other cells

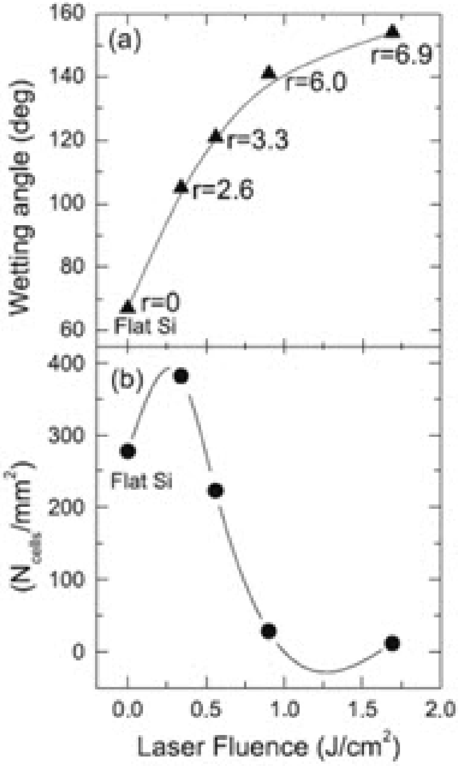

Figure 5.3: (a) Relation between the laser fluence and surface wettability for the series A patterned Si substrates; the corresponding roughness ratio for each sample is also indicated; (b) cell density after 72h incubation as a function of the surface wettability for the flat Si and structured surfaces of series A. All experiments are done on triplicates and the cell density values plotted are the calculated mean values. The lines serve as a guide for the eye.

to populate that region, resulting in the formation of cell multi-layers (Figure 5.4 (f)). The extent of cell spreading on a material provides a visual qualitative indicator of the strength of the cell-surface interaction. [87] Polygonal cell spreading implies extensive interaction between the surface and the cells, whereas weak cell-surface interaction results in cell clustering. [87]

Cell viability of the attached cells on the different surfaces is assessed using the live-dead kit (Figure 5.5). This staining protocol facilitates counting the number of live (depicted as green) and dead cells (depicted as red/yellow) per unit area. According to this test cell cultures on hydrophilic surfaces (A1) represent a very low percentage of dead cells, equal to 2%. This percentage seems to increase proportional to the roughness ratio, namely on surfaces A2 and A4 the particular percentages are 17% and 42%, respectively. The corre-

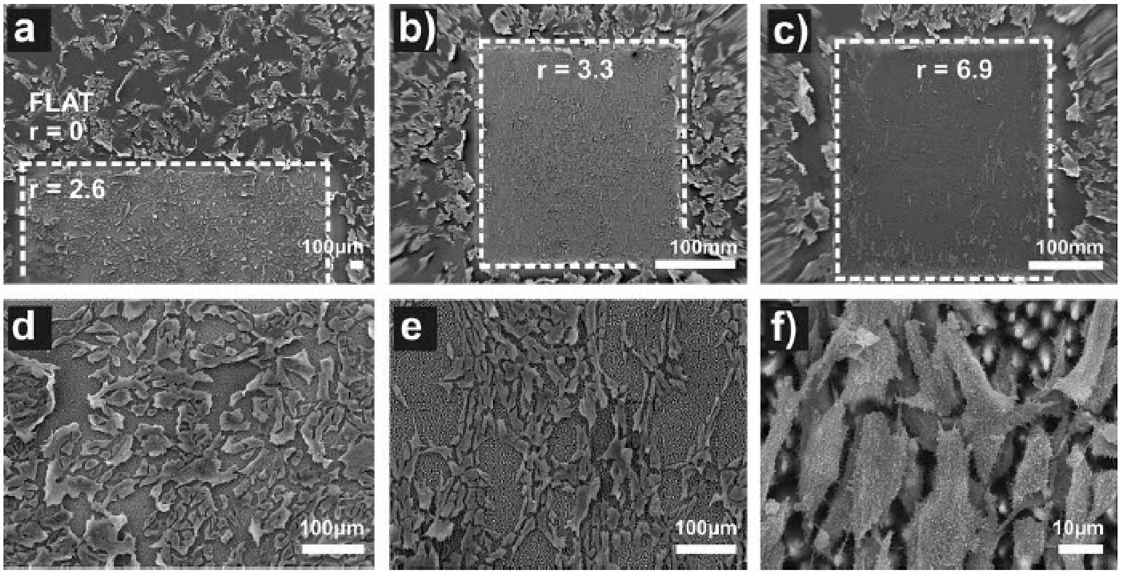

Figure 5.4: SEM micrographs of NIH/3T3 cells cultured on flat (a) and A1 (a and d), A2 (b and e), A4 (c and f) patterned Si substrates with low, mid and high roughness ratio respectively. The corresponding roughness ratios are also shown. The dashed lines indicate the border between flat and patterned regions.

sponding dependence of the live cell density on the laser fluence and surface wettability is presented in Figure 5.3 (b) and Figure 5.6, respectively. It is obvious that the induction of roughness facilitates cell spreading up to an optimum roughness ratio. On the contrary, cell spreading is inhibited on highly rough and super-hydrophobic substrates.

Furthermore, hydrophobization of substrates using a hydrophobic silane

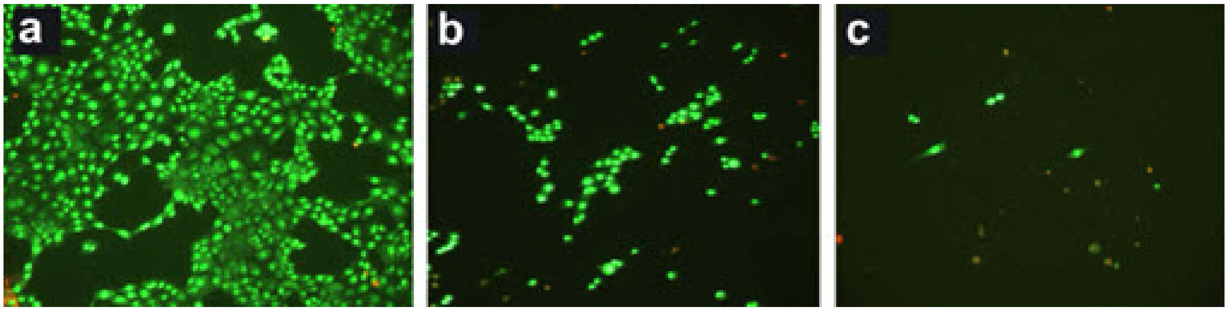

Figure 5.5: Fluorescence microscopy images of live (green) and dead (yellow-red) cells cultured on A1 (a), A2 (b) and A4 (c) patterned Si substrates.

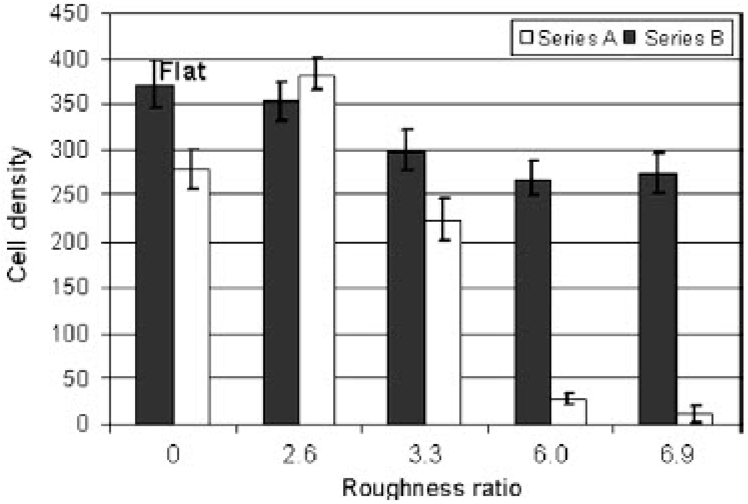

Figure 5.6: Cell density of fibroblasts on flat and oxidized Si, the as-prepared (series A) and oxidized (series B) patterned Si surfaces after 72h incubation. All experiments are done on triplicates and the cell density values shown are the calculated mean values.

coating, fails to reverse the inhibition of cell spreading. In order to further characterize the principal surface property determining cell response, the wettability of the substrates can be modified by coating the structures with a hydrophilic oxide layer. As a result, all the structured surfaces are converted to super-hydrophilic, without altering their initial morphology (Figure 5.7 (a)). In this case, a remarkable change in cell behavior is obtained, since they spread well in the highly rough oxidized surfaces, B3 and B4 (Figure 5.7 (b)). Similar results are obtained by culturing HeLa cells on the above mentioned surfaces (data not shown).

Following the corresponding evolution of cell densities for the hydrophobic and hydrophilic surface chemistries (Figure 5.6 and Figure 5.8), it can be argued that the cell response is not solely dependent on surface morphology or surface chemistry, but on their combination, which represents surface energy. Thus, fibroblasts preferentially adhere to high surface energy or hydrophilic substrates. The ability to tune the surface energy of the patterned Si substrates, by changing either the total roughness or chemistry, could allow advantageous manipulation of the cell behavior and vice versa.

Cell adhesion

Once fibroblasts detect their target location using the filopodia on their leading edge, the formation of lamellipodia facilitates the cell movement to

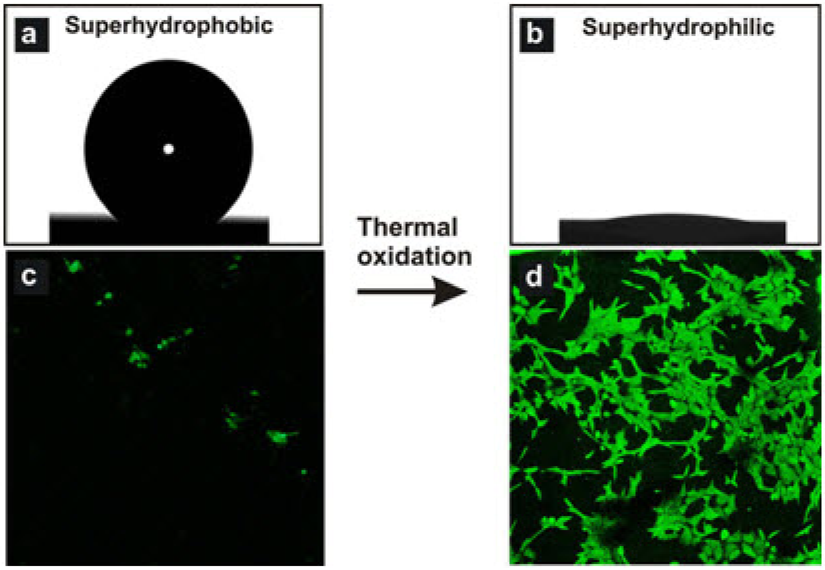

Figure 5.7: Images of water droplets placed on: (a) the roughest patterned Si surface (A4) and (b) on the same surface coated with a hydrophilic silicon oxide layer (B4). The corresponding confocal microscopy pictures of fibroblast cells cultured for three days on these surfaces are also shown. After thermal oxidation, the super-hydrophobic substrate becomes super-hydrophilic. As a direct consequence, the culture substrate switches from fibroblast-phobic to fibroblast-philic.

the desired site. [93] While a lot of studies have reported that cells are sensitive to micro/nanoscale topography [90, 91], it is generally accepted that cells use filopodia for spatial sensing in their movement and spread on structured surfaces. Thus, the ability of fibroblast cells to recognize and adhere to the different surfaces described here is, also, examined.

Confocal microscopy analysis, following actin distribution in the cells growing on the different structured surfaces, clearly shows morphological changes in the various cases tested here (Figure 5.9). Thus, fibroblast cells growing on more hydrophobic surfaces are mostly rounded (Figure 5.9 (g) and (i)), while a significantly larger number of cells growing on that surface (Figure 5.9 (c) and (e)) as well as on flat control (Figure 5.9 (a)) produce lamellae. In all cases the actin filaments are located at the cell periphery. The high magnification SEM images confirm the differences in lamellipodium formation, also showing that cells on less hydrophobic structured areas are polarized with areas of dense filopodia extension (Figure 5.9 (d) and (f)). Some of these cells are showing a kind of flattening, but reduced size as compared to cells growing

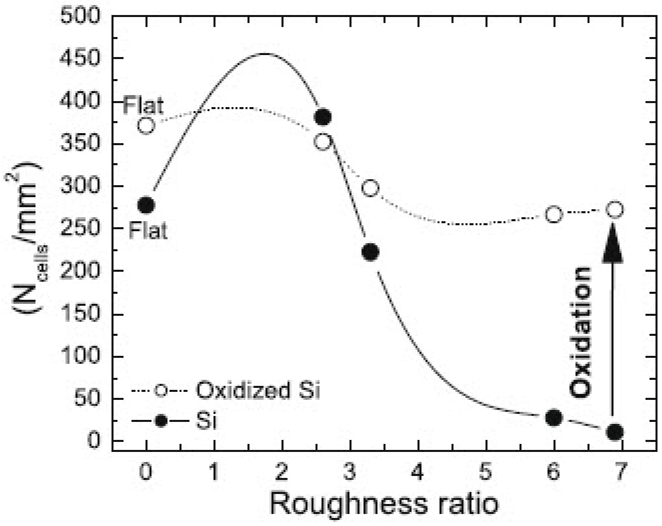

Figure 5.8: Relation between cell adhesion and surface wettability for the flat and patterned Si surfaces of series A and series B. All experiments are done on triplicates and the cell density values plotted are the calculated mean values. The lines serve as a guide for the eye.

on the flat controls (Figure 5.9 (b)). These processes are spread in multiple planes perpendicular to the patterned area, suggesting a 3D cell proliferation mode (Figure 5.9 (d) and (f)). On the contrary, cells growing on the super-hydrophobic surfaces seem to be smaller, with decreased number of filopodia extensions. This type of morphology could therefore be used to assess the quality of cell-surface interactions. Furthermore, the numeral processes developed between cells should facilitate cell-cell interaction and communication.

In order to evaluate the ability of fibroblasts to adhere on 3D structured surfaces, the expression of vinculin protein is examined. The membrane expression of vinculin, which is a member of focal adhesions molecules, indicates the existence of strong cell-substrate adhesion. As shown in Figure 5.10, vinculin is expressed in fibroblasts cultured on A1 surfaces (Figure 5.10 (a)) and co-localized with actin at the edges of filopodias (Figure 5.10 (c)). Similar results are obtained after double staining of cells cultured on the highest roughness ratio oxidized substrates (B4). On the other hand the weak cell-substrate adhesion on super-hydrophobic surfaces is evidenced by the low vinculin expression (A4; Figure 5.10 (d)).

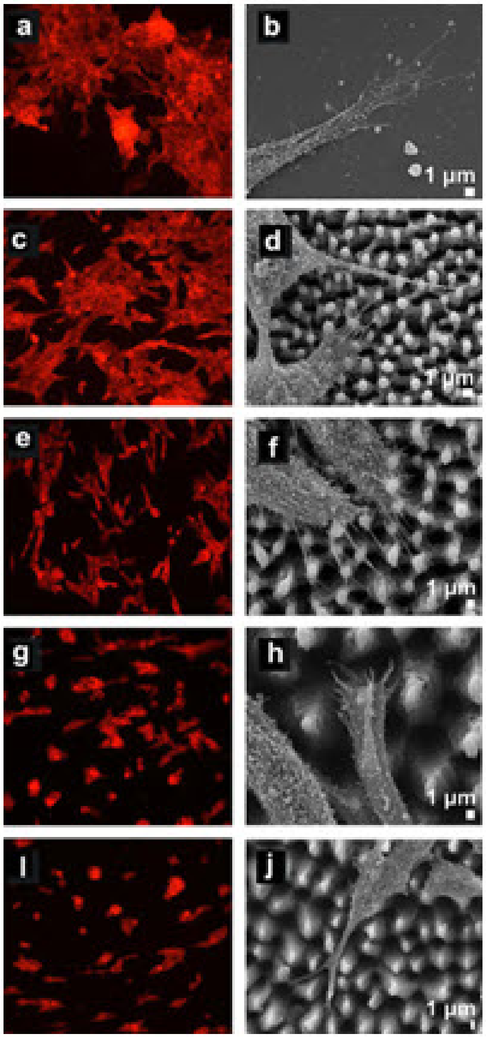

Figure 5.9: Fluorescent microscopy images of fibroblasts, showing actin cytoskeletal networks on flat silicon surface (a) and on patterned surfaces (c, e, g, and i). The corresponding SEM micrographs of fibroblast cell adhering to flat (b) and to patterned surfaces (d, f, h, and j) are also shown; (c and d: A1 surfaces; e and f: A2 surfaces; g and h A3 surfaces; l and j: A4 surfaces).

5.2.4 Discussion

The fibroblast cell response on the three-dimensional silicon-engineered surfaces can be simply explained. The physical behavior of hydrolyzed living cells may be regarded as a drop of liquid. The adhesion of this cell liquid can be affected by the surface wettability due to the increased or decreased contact area, which is proportional to the solid-liquid interfacial adhesive force. Alter-

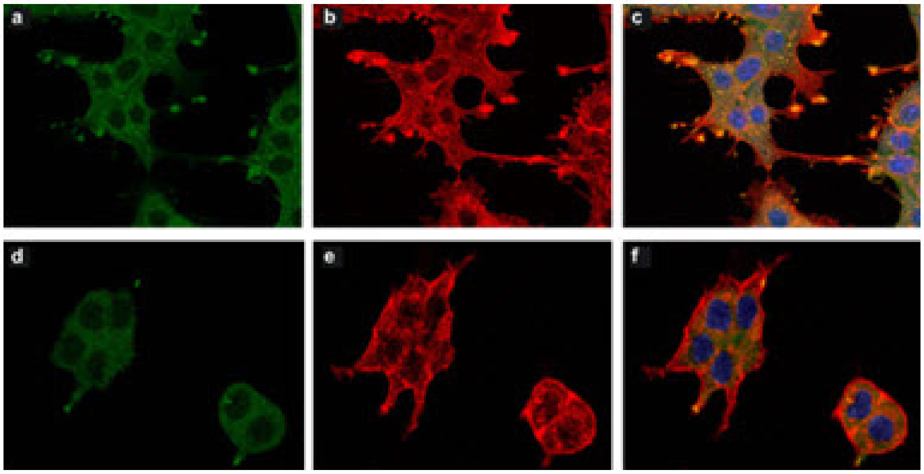

Figure 5.10: Confocal images showing the distribution of actin (red) and vinculin (green) in fibroblasts cultured for 3 days: (a-c) on the low-rough patterned surface (A1), (d-f) on the highly-rough patterned surface (A4). Double stained images are also shown.

natively, a living cell can be described by tensegrity models [92] which consider that cellular shape and adhesion are largely influenced by the cytoskeleton; the cell tends to form focal adhesions in locations that balance cytoskeletal forces. In this respect surface wettability is crucial as it describes to what extend the surface is exposed to culture medium and subsequent protein adsorption. A reduction in adhesive protein adsorption due to a decreased liquid-surface interfacial area may detrimentally affect the ability of cells to form adhesions. In any case, the surface energy influences the contact area of the cell membrane with the substrate, while the profile of membrane could change depending on the wettability of the adjacent solid.

Following the results presented in Figure 5.3(a), it is obvious that the wetting angle values measured for the structured substrates are consistent with the Cassie-Baxter model because, in contrast to the Wenzel model, it predicts a rise in the WA upon enhancement of the roughness of an initially hydrophilic ($\theta > 90^o$) surface. Hence, for the super-hydrophobic substrates, where the solid-liquid contact area is minimal, water cannot penetrate the roughness elements and therefore an intervening air layer persists.

This air layer is visible at non-zero reflection angles and is responsible for the silvery underwater reflections from aquatic species. Indeed, as shown in Figure 5.11, when a water repellent spike-substrate is immersed in water or cell culture liquid, it glistens with a silvery sheen, indicating that a sheathing film of air remains on the submerged surface. Conversely, for more hydrophilic substrates, the fraction of the wetted area increases and the surface glistening disappears, as a result of increasing liquid penetration. Finally for super-hydrophilic substrates, the contact area is maximized and water completely penetrates the roughness elements. Therefore, taking into account that cell culture medium is aqueous, the interaction of cell membrane with the underlying substrate may be governed by the degree of surface wettability and thus surface energy.

Fibroblast spreading is promoted on hydrophilic or high surface energy rough substrates due to the permeation of the culture liquid in the structures, allowing cells to take advantage of the high surface-area-to-volume ratio offered by the structured substrates. On the contrary, fibroblast adhesion is almost impossible on ultra-hydrophobic or low surface energy rough substrates, as the penetration of the culture liquid on the structures is inhibited.

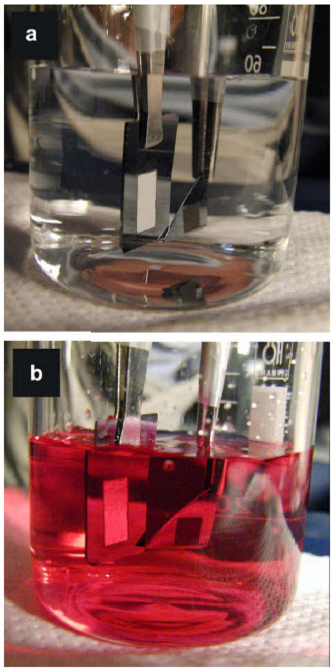

Figure 5.11: Pictures of the as-prepared super-hydrophobic (sample A1, on the left) and oxidized super-hydrophilic (sample B4, on the right) patterned regions immersed in water (a) and cell culture medium (b) respectively. The silvery shine is visible only on the super-hydrophobic patterned region of the A1 sample while it is absent on flat regions and the less hydrophobic patterned area of the B4 sample.

5.3 Functionalization of laser microstructured Si

5.3.1 Introduction

The covalent attachment of small organic molecules and larger functional biomolecules such as DNA, enzymes or other proteins on semiconducting materials is a new field of basic and applied research with an interdisciplinary interest. The ultimate goal of this research effort is the formation of organic/inorganic heterostructures which can provide a direct link between biology and semiconductor technology on both micrometer and nanometer lengthscale. Hybrid structures, such as heterointerfaces between organic and inorganic materials, have attracted the attention of basic and applied sciences due to their potential applications in the field of bio-nanoelectronics and tissue engineering. The perspective is that the organic/inorganic heterostructures will be able to perform specific biological functions better than either purely organic or purely inorganic structures. [73]

On the organic side, small organic molecules, specific biomolecules and bioentities (i.e. peptides) and living cells could be of great interest for such hybrid structures. On the inorganic side, metals, semiconductors and insulators could be possible candidates. However, because of their potential advantages and their technological maturity, semiconductors as functional biomaterials have been developed into a very active field at the interface between physics, chemistry and biology. Therefore, silicon, as the workhorse of semiconductor materials, has received most of the attention among all semiconductors in the field of biointerfacing. Apart from the advanced use of the MOSFET technology in Ion Sensitive Field Effect Transistors (ISFETs) for interfacing with neuronal networks for example, silicon has also been used as a substrate for the covalent, chemical attachment of small organic molecules.

Ideally, the biomolecules are covalently immobilized on the clean surface of the substrate via suitable linker molecules. The main role of the linker molecules is to provide a high density of docking sites for the specific attachment of biomolecules and at the same time, to maintain a sufficiently low density of electronic defects on the semiconductor surface. Otherwise, this would have a negative impact on the electronic properties of the heterostructure. Such heterojunctions should maintain both their biological and electronic functionality. [73]

A variety of functionalization techniques have been developed for rendering the interface of semiconducting surfaces to biological systems more stable and biocompatible. Most of these approaches make use of the formation of self-assembled organic monolayers (SAMs) or multilayers on clean surfaces. An approach for the functionalization of silicon and also other semiconductors still covered with a certain fraction of native oxides is the silanization scheme, which is widely employed for the functionalization of glass, quartz substrates, and for Si/SiO_2-MOSFET devices. In this case, the semiconductor surface is treated in a specific way to optimize the surface coverage with hydroxyl (-OH) groups. Subsequently, the OH-terminated surface is exposed to alkoxysilanes such as APTES (3-aminopropyl- triethoxysilane) under conditions optimized for the formation of a dense, self-assembled APTES monolayer covalently bonded to the Si surface oxide by Si-O-Si bridges. Finally, small biomolecules can be attached to the functional end groups of the APTES terminated surface.

In this section, the functionalization of microstructured sillicon exhibiting surface roughness both at the micrometer and nanometer length-scale is examined. The silicon microstructures are laser-fabricated under reactive gas atmosphere. Next, the silicon samples, possessing conical structures on their surfaces, are subjected to the appropriate chemical treatment, which includes surface oxidation, APTES-silanization and gold coating. After the chemical modification, the last step is the covalent attachment of fibrous peptides on the activated Si surfaces. In the first part of this chapter, we discuss about the formation of self-assembled monolayers (SAMs) on solid surfaces and, in particular, the formation of APTES monolayers. Furthermore, we see some useful details about the fibrous peptides. Finally, the covalent attachment of such fibrous peptides on the Si microstructures is investigated.

5.3.2 Self-assembled monolayers (SAMs)

A self-assembled monolayer (SAM) is an organized layer of amphiphilic molecules in which one end of the molecule, the head group shows a special affinity for a substrate. SAMs also consist of a tail with a functional group at the terminal end as seen in Figure 5.12. SAMs are created by the chemisorption of hydrophilic head groups onto a substrate from either the vapor or liquid phase followed by a slow two-dimensional organization of hydrophobic tail groups. Initially, adsorbate molecules form either a disordered mass of molecules or form a lying down phase, and over a period of hours, begin to form crystalline or semi-crystalline structures on the substrate surface. The hydrophilic head groups assemble together on the substrate, while the hydrophobic tail groups assemble far from the substrate. Areas of close-packed molecules nucleate and grow until the surface of the substrate is covered in a single monolayer. Adsorbate molecules adsorb readily because they lower the surface energy of the substrate and are stable due to the strong chemisorption of the head groups. [68]

The selection of the type of head group depends on the application of the SAM. Typically, head groups are connected to an alkyl chain in which the terminal end can be functionalized (i.e. adding -OH, -NH_3, or -COOH groups) to vary the wetting and interfacial properties. An appropriate substrate is chosen to react with the head group. Substrates can be planar surfaces or roughened surfaces. The nature in which the tail groups organize themselves into a straight ordered monolayer is dependent on the inter-molecular attraction, or Van der Waals forces, between the alkyl and tail groups. To minimize the free energy of the organic layer the molecules adopt conformations that allow high degree of Van der Waals forces with some hydrogen bonding. . [68]

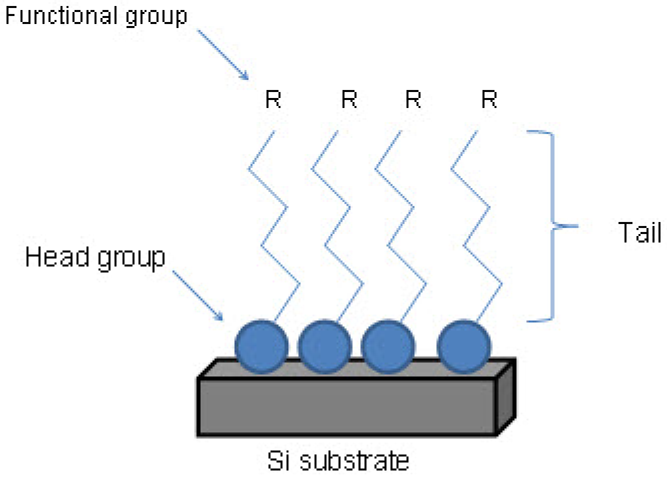

Figure 5.12: Schematic of self-assembled monolayer.

SAMs are an inexpensive and versatile surface coating for applications including control of wetting and adhesion, chemical resistance, biocompatibility, sensitization and molecular recognition for sensors. Areas of application for SAMs include biology, electrochemistry and electronics, nanoelectromechanical systems (NEMS) and microelectromechanical systems (MEMS), and everyday household goods. SAMs can serve as models for studying membrane properties of cells and organelles and cell attachment on surfaces. SAMs can also be used to modify the surface properties of electrodes for electrochemistry, general electronics, and various NEMS and MEMS. Another application of SAMs is the functionalization of biosensors. The tail groups can be modified so they have an affinity for cells, proteins, or molecules. The SAM can then be placed onto a biosensor so that binding of these molecules can be detected.

Significant attention has been drawn towards the modification of materials surface by forming such ordered monomolecular organic films. One effective way to form such thin films is by the simple immersion of the materials substrates into a solution containing functional organic molecules. These organic films are known as self-assembled monolayers (SAMs) and they are formed spontaneously. The most attractive feature of SAMs is molecular level control over the modification of surfaces, and the incorporation of multiple or multilayer molecular components onto the monolayer leads to a wide range of functional properties.The most commonly employed examples are alkylsiloxane monolayers, fatty acids on oxide monolayers and alkanethiolate monolayers. [55, 56]

In particular, SAMs formation provides a means of surface functionalization by organic molecules containing suitable functional groups like -SH, -CN, -COOH, -NH_2 and silanes on metallic (Au, Cu) as well as semiconducting surfaces (Si, GaAs). [57] This means that SAMs can be prepared using different types of functional molecules and different substrates. The first types of strongly bound chemisorbed monolayers using silane compounds were reported by Sagiv, where glass or oxidized silicon surfaces were coated with active silanol groups. Nowadays, research interest is directed towards the implementation of SAMs with terminal amine groups which have the capability of attaching larger molecules, and in particular biomolecules, such as enzymes, proteins, DNA, etc. [58–60] The terminal functionalities of the organic molecules bound on the substrates affect the wetting behavior (hydrophobicity/hydophilicity) of the underlying surfaces.

Next, the self-assembly of silane molecules onto materials surface is discussed. Aminosilanes such as (3-Aminopropyl)-triethoxysilane (APTES) are widely used, especially, for biological applications and, thus, more emphasis is given to this type of silane.

Silane self-assembled monolayers

Silane is a chemical compound with the chemical formula SiH_4. It is the silicon analogue of methane. More generally, silane is any silicon analogue of an alkane hydrocarbon. Silanes consist of a chain of silicon atoms covalently bonded to each other and to hydrogen atoms. They tend to be less stable than their carbon analogues because the Si-Si bond has a strength slightly slower than the C-C bond. Furthermore, oxygen decomposes silanes easily, as the silicon-oxygen bond is thermodynamically more favored than the Si-Si bond. Another property of silanes is that they can incorporate the same functional groups (-OH, -NH_2, etc.) as alkanes, i.e. -OH in order to make a silanol (a hydrogen atom is removed and a hydroxyl substituent binds diretly to the silane chain). Silanols are similar to alcohols just as silanes are similar to alkanes, and they are, mainly, synthesized by hydrolysis of aminosilanes.

Silanization is the covering of a solid surface with silane-like molecules. Mica, glass and metal oxides can all be silanized, as they contain hydroxyl groups which attack and displace the alkoxyl groups on the silane, and thus forming a covalent Si-O-Si bond (siloxane bond). In silanization processes, more complex silane molecules are used. The hydrogen atoms can be repalced from alkoxyl groups and the alkoxysilanes are obtained. In chemistry, an alkoxyl group is an alkyl group (carbon and hydrogen chain) linked to oxygen, thus R-O. The range of alkoxyl groups is great, the simplest being methoxy with chemical formula, -OCH_3 (the ethoxy group is the -OCH_2CH_3). The goal of silanization is to form bonds across the interface between mineral components and organic components. The organofunctional alkoxysilanes are classified according to their organic functions. The organic function can be a primary or secondary amine which corresponds to aminosilanes (APTES, Figure 5.13) or it can be an epoxide corresponding to glycidoxysilanes (GPMES) or it can be a thiol which corresponds to mercaptosilanes.(MPTS, MPDMS)

A very important and interesting goal of the silanization of solid substrates is the covalent attachment of biomolecules (proteins, DNA) onto their surfaces. The biological functionalization of the surfaces can be achieved by depositing and coating the surface with silane containing an amino-group. Once the amine groups are available, as this method provides high density of them on the deposited surfaces, numerous cross-linking agents can be used to further promote immobilization of biomolecules.

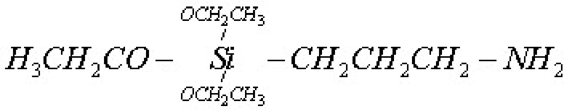

$$H_3CH_2CO-\overset{OCH_2CH_3}{\underset{OCH_2CH_3}{Si}}-CH_2CH_2CH_2-NH_2$$

Figure 5.13: The APTES molecule.

APTES self-assembled monolayers

3-Aminopropyltriethoxysilane (APTES) is one of the most frequently used organosilane agents for the preparation of amino-terminated films on silicon substrates. A general consensus regarding the APTES film formation is that silanization begins with the hydrolysis of ethoxy groups in APTES, a process catalyzed by water, leading to the formation of silanols. APTES silanols then condense with surface silanols (surface hydroxyl groups) or with other silanol groups on neighboring silanes forming a monolayer of APTES via a lateral siloxane network in which amino groups are oriented away from the underlying silicon surface. Many experimental results, however, have suggested that this is an oversimplified description of the idealized reaction and the actual process is far more complex and sensitive to reaction conditions. [61] The ideal silanization process for all reaction stages is sketched in Figure 5.14. [67]

The complexity of the APTES silanization reaction mainly stems from the presence of a reactive amino group in APTES and its inherent propensity to enter into competing reactions. The amino groups in adsorbed APTES interact with silanols present on the silicon surface and/or in the adjacent hydrolyzed APTES via hydrogen bonding or electrostatic interactions. [62, 63] This considerably reduces the number of available silanol groups on both the silicon surface and the APTES for further siloxane condensation. In addition, polymerization of APTES gives rise to the formation of multiple APTES layers whose structures and reactivity are likely different from those of an APTES monolayer.

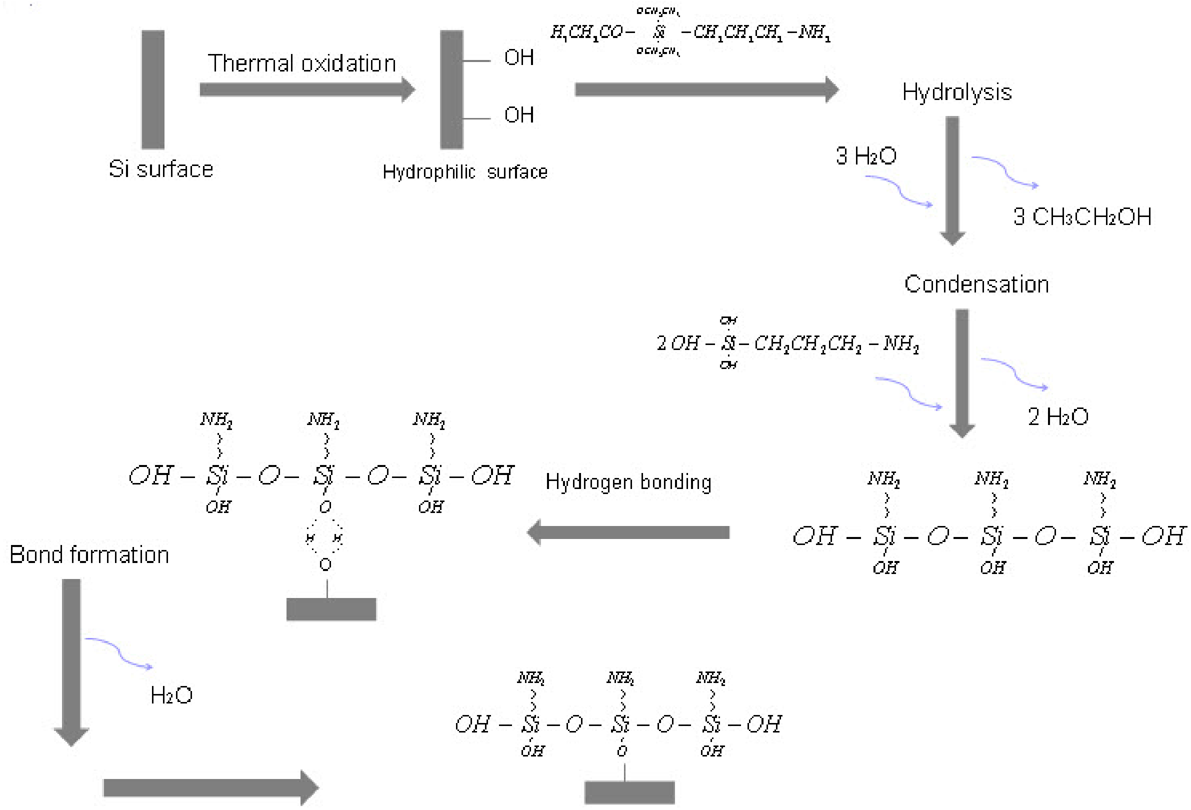

Figure 5.14: Schematic of APTES silanization process.

In general, the structure and properties of the silane layer on a solid surface depends on the functionality attached to the silane, but also on the method used to apply the silane to the surface. The ideal case would be to form a monolayer of coupling agent to the surface where all silanol groups have reacted either with surface hydroxyl groups or silanol groups on neighboring silanes.These are significant issues when preparing APTES films since the availability and the reactivity of surface amino groups are crucial to many applications including the construction of silicon-based biomedical microdevices. [64]

APTES films on silicon substrates can be characterized by multiple analytical techniques including X-ray photoelectron spectroscopy (XPS), Fourier Transform infrared spectroscopy (FTIR), ellipsometry and contact angle measurements. Ellipsometric measurements and FTIR spectra provide valuable information about the structure and thickness of the formed APTES films. Contact angle data give indications about their wettability. In addition, the reactivity of the the amine groups on APTES films can be estimated by fluorescence measurements. In general, the properties of the APTES films depend strongly on the preparation conditions such as the deposition time and the choice of reaction solutions due to differences in the APTES adsorption process and film growth mechanisms. [65]

In our study, a contact angle analysis is used as it provides a quick and simple means of assessing the reactivity of the surface and allows for general comparisons providing a qualitative test. Changes in surface topology influences the contact angle measurements from a macroscopic point of view. However, the contact angle results cannot distinguish between monolayer and multilayer coverage and cannot give information about the thickness of the resulting APTES layers.The only information provided from the contact angle data is that the silanized surface becomes more hydrophobic as the APTES film thickness increases. [65]

5.3.3 Amyloid fibrous assemblies

Amyloid fibrils are insoluble fibrous protein aggregates which are organized in a specific way and share specific morphological and structural properties. Abnormal accumulation of amyloids in organs may lead to amyloidosis, and may play a crucial role in various other degenerative diseases. The term amyloid is referred to proteinaceous assembly comprising unbranched long fibrils. In general, many proteins or peptides can form amyloid fibrils and, thus, there is not a specific protein associated with amyloid assemblies.

Amyloid assemblies can also be formed by proteins and peptides that do not participate in the onset and evolution of a disease as a result of misfolding and/or misassembled events [69]. Morphologically, amyloid fibrils have a width of about 10nm and length ranging from 1 to 10μm (Figure 5.15) [70]. They are visible with Transmission Electron Microscopy and Scanning Electron Microscopy. The internal structure of the fibril is composed of several β-strands perpendicular to the axis of the fibril [70]. These structures are generally identified by gold-green birefringence when stained with congo red and seen under polarized light.The synthesis of such proteins or peptides in vitro is feasible, and therefore the study of the early stages of their self-assembly as well as their behavior after the formation of the fibrils is achieved.

A wide range of amyloid assemblies are studied for biological and nanotechnological applications constituting a novel field, named bio-nanotechnology.

Figure 5.15: Morphology of amyloid fibrils (scale bar: 100nm).

Adenovirus fibers as a self-assembly system

A distinct class of fibrous proteins is adenovirus fibers that are used as attachment organelles by viruses. Octapeptides derived from this type of fibrous protein can be used in various biological applications [71]. It was shown that a sequence of 8 or 6-residue peptides can form amyloid fibrils. These peptides may, therefore, self-assemble into a fibrous cross-beta structure, with the beta-strands being perpendicular to the fibril axis.

Inspired from this model, Kasotakis et al synthesized new octapeptides in order to study their fibril-forming ability, their morphology and their potential use on bionanotechnological applications. They used a natural self-assembly natural building block as a scaffold and modified it in order to endow it with additional functionalities. They chose the 8-amino acid peptide as the starting building block, N-S-G-A-I-T-I-G. This peptide corresponds to a region in the adenovirus fiber protein sequence. Then, they opted to synthesize two new octapeptides by substituting new amino acids only at specific positions.(Figure

5.16)

In particular, the new designed peptides obtained metal binding affinity by incorporating cysteines in the sequence of the residues. Cysteine is the most common metal binding amino acid. One of the new peptide sequences is the N-C-G-A-I-T-G, where cysteine (Cys) substitutes serine (S). A different peptide sequence is N-A-G-A-I-T-G, where alanine (A) substitutes serine (S). The amino acid sequence of the octa-peptides with their code names is shown in Table 1.

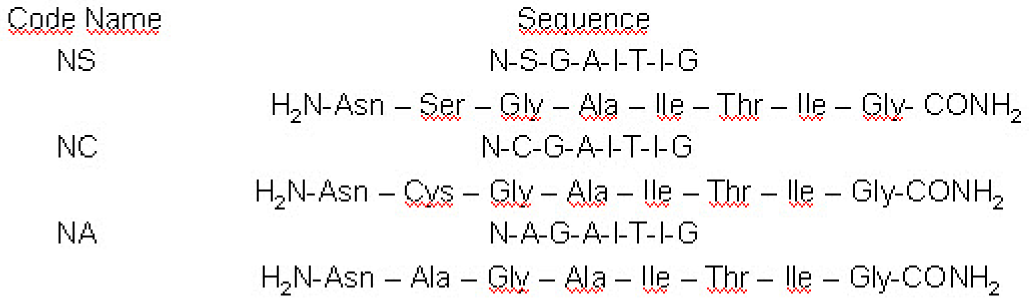

Code Name	Sequence
NS	N-S-G-A-I-T-I-G H_2N-Asn – Ser – Gly – Ala – Ile – Thr – Ile – Gly- $CONH_2$
NC	N-C-G-A-I-T-I-G H_2N-Asn – Cys – Gly – Ala – Ile – Thr – Ile – Gly-$CONH_2$
NA	N-A-G-A-I-T-I-G H_2N-Asn – Ala – Gly – Ala – Ile – Thr – Ile – Gly-$CONH_2$

Figure 5.16: Sequence of the 8-amino acid peptides.

The peptides, having a degree of high purity are, initially, in the form of a powder and, then, they are dissolved in appropriate buffer solutions. Depending their concentration and days of incubation, the peptides are self-assembled and obtain the characteristic structure and morphology of amyloid fibrils. The structural characterization of the amyloid fibrils is performed with Transmission Electron Microscopy. The peptide NS exhibits characteristic amyloid fibrillar morphology. It forms very long thin fibrils with the size ranging from 10 to 40nm width; the fibrils can reach up to 50μm in length. The NC peptide possess, also, amyloid type morphology with a size varying between 20 and 35nm in width; the length can reach several micrometers. [72] Similar features are observed at the NA peptide.

Application of amyloid fibrils

Self-assembling peptides, which can be characterized as bioinspired fibrous materials, may have potential applications in the emerging field of bionanotechnology, particularly due to the interesting advantages they offer; they are synthesized and manipulated easily and they are highly stable. Furthermore, their specific structure and morphology have been extensively studied and, more significantly, their chemistry can be adjusted concerning their potential biological use. [3]

In this work, we examine the attachment of fibrous self-assembling peptides on the laser-assisted microstructured Si surfaces, constituting our inorganic substrates. The combination of peptide self-assembling features with chemistry can lead to peptide binding on highly rough three-dimensional silicon surfaces with gradient roughness ratios and wettabilities. In addition, fibrous peptides can be potentially enriched with functional moieties, such as cell adhesion factors, and their immobilization to the roughened surface of silicon substrates can enhance the adhesion and the viability of tissue-forming cells. As a consequence, the micro-structured silicon samples may be biofunctionalized and they can be used as three dimensional scaffolds for cell attachment and growth.

The micro-patterned Si surfaces should be chemically modified in order to bind the amyloid fibrils. In this work, the used peptides are self-assembled octapeptides derived from sequences of a natural fibrous protein, the adenovirus fiber, as previously described We use the octapeptides NCGAITIG (NC) and NAGAITIG (NA) which are variants of the peptide NSGAITIG and self-assemble into amyloid-type fibrils in solution. The method which we use for the functionalization of our microstructured substrates is described in the next subsection.

5.3.4 Functionalization of Si microstructures

Experimental procedure

Single crystal n-type silicon wafers (100) or microstructured silicon substrates are cleaned in a 10 minute trichloethylene, followed by a 10 minute acetone, followed by a 10 minute methanol bath, prior to chemical modification, in order to clean the organic residues off the samples' surface. The samples are, then, thoroughly rinsed in a deionized (DI) water cascade with three baths, 5 minute each bath. The Si samples are then treated with 40% hydrofluoric acid for 90 minutes in order to remove the native oxide layer grown on their surface. Next, the substrates are rinsed again in the three deionized water baths for a 5-minute duration in each bath and, finally, they are blown dry with nitrogen. The silicon substrates are immediately subjected to chemical modification.

The carefully cleaned substrates are covered with a thermally grown oxide layer which provides high density of hydroxyl groups onto their surface. For thermal oxidation, the samples are placed in a box furnace and heated at 1000 °C for 30 minutes in air. The oxidized samples are then immersed into a solution of 30ml anhydrous toluene containing 0.5ml 3-aminopropyltriethoxysilane (APTES) and silanization takes place. The oxidized samples are incubated in the above solution at 120 °C for 3 hours, and the amine group derivatization of silicon wafers is carried out. After the reaction time, the Si substrates are washed in succession with chloroform (5 minutes), acetone (5 minutes), methanol (5 minutes), and extensively with water (5 minutes) in order to remove the non-covalently absorbed silane molecules. The silanized substrates are dried with nitrogen. The APTES-modified Si substrates provide reactive surface amine groups which are positively charged.

The following step of the functionalization scheme is the gold coating of the silanized substrates. For this, hydrogen tetrachloroaurate, an inorganic compound with the molecular formula $\mathrm{HAu}Cl_4$, is used as a precursor to gold. $\mathrm{HAu}Cl_4$ looks like golden yellow crystals and it is hygroscopic.When it is diluted in water, $\mathrm{HAu}Cl_4$ consists of the square planar $[\mathrm{Au}Cl_4]^-$ ion and the proton is associated with water. This property is exploited and $\mathrm{HAu}Cl_4$ is diluted in water at a concentration of 0.1gr/400μl. A small droplet of this solution is deposited onto the samples for 40 minutes. The substrates are, then, rinsed twice with deionized water in order to remove the non-bound gold. The gold, being negatively charged, binds electrostatically to the positively charged amine groups and, thus, form a uniform layer on the Si samples. The gold layer formed on the Si substrates plays the role of the cross-linker between the APTES-modified Si substrates and the peptide fibrils.

For the experiments, aqueous peptide solutions at a concentration of 2 mg/ml and aged for a few days are used. The peptide solutions have been aged so that self-assembled fibrils have already been formed in solution (reaching the order of microns in length). A droplet of the peptide solution is spread onto the micro-patterned and flat substrates. The attachment of the peptides fibrils on the gold coated surfaces takes place. This is achieved through the thiol group (-SH) of the peptide fibrils provided by the cysteine amino acid (Figure 5.17, which adsorbs on the gold coated surfaces and the strong covalent bond (S-Au) is formed. The peptide solutions are incubated on the silicon substrates for 2 hours at room temperature. The samples are subsequently washed three times with water .

Cysteine-containing peptide fibrils (NC) are expected to bind to the chemically modified Si surfaces due to thiol chemistry. On the other hand, the use of peptide solutions that do not contain cysteine in their sequence seems to be necessary, since such peptides are not able to be attached on the gold-coated silicon samples and, thus, they can serve as a control test.

Schematically, the method followed for the covalent attachment of the peptide fibrils on the Si samples is depicted in Figure 5.18

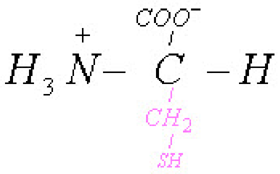

$$H_3\overset{+}{N}-\overset{COO^-}{\underset{\underset{SH}{CH_2}}{C}}-H$$

Figure 5.17: The cysteine molecule.

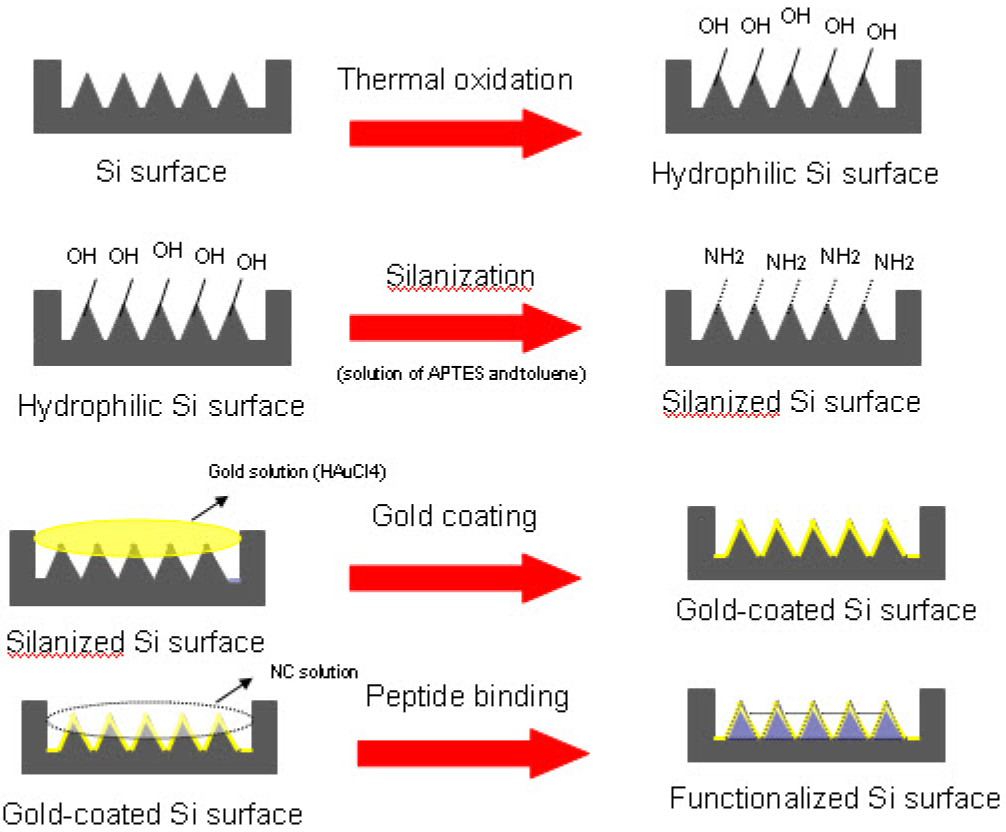

Figure 5.18: Functionalization scheme of Si substrates.

Experimental results

In the previous part of the work, the experimental procedure for Si functionalization and peptide binding is demonstrated. NC peptide is expected to be bound onto Si substrates due to thiol chemistry, whereas the NA peptide is not. These assumptions are confirmed by the experimental results. After the aforementioned treatment, Si samples are covered with 10nm gold using the sputtering technique so that they can be visualized with scanning electron microscopy. Firstly, flat Si substrates coated with gold are immersed in an aqueous solution of peptides that contain the cysteine residue (NC peptide). Self-assembled NC fibrils are already formed in solution. A thin layer of peptides will form on the Si samples (Figure 5.19). On the other hand, no peptide attachment is observed in the case of the NA peptide.

Next, the same procedure is followed, also, for the microstructured Si substrates exhibiting gradient roughness ratios. Peptide conjugation onto structured Si samples is achieved for three different roughness ratios: low, mid and high (Figure 5.20, Figure 5.21 and Figure 5.22respectively. During the peptides incubation on the silicon substrates, a thin layer of peptides is formed on the microstructures and the fibrils further grow on them. In particular, at low roughness (Figure 5.20(a), (b), (c) and (d)) a network of peptide fibrils is created among neighboring Si spikes. This network consists of peptide ”bridges” which link the Si pillars.

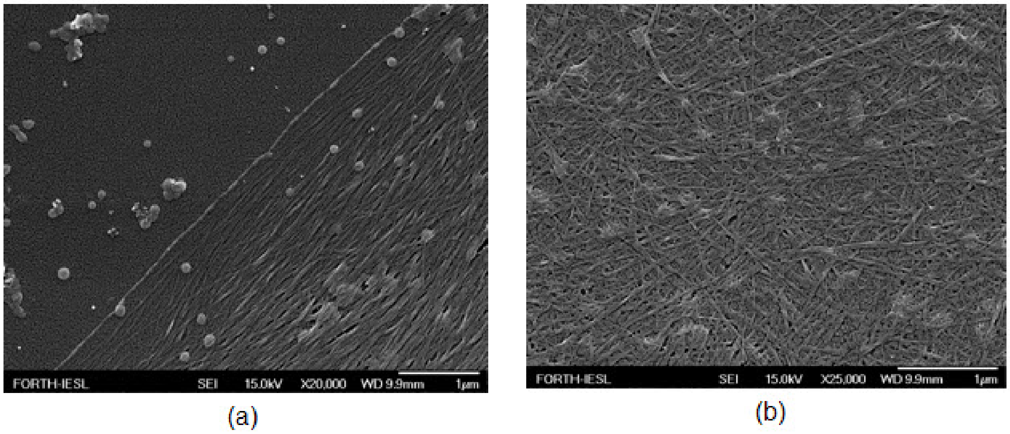

(a) (b)

Figure 5.19: SEM images of flat Si sample coated with self-assembled NC fibrils (a) at the border and (b) in the center of the peptide (NC) solution droplet.

At mid roughness, from the SEM images, it is obvious that peptides bridges are, also, self-assembled between the silicon microstructures. These peptide bridges can link not only the tops of the Si cones (Figure 5.21 (a) and (b)) but also, the top of one cone with the base of another one (Figure 5.21 (a), (c) and (d)). For the fibril bridge to form, a thin layer of peptides should be formed on the 3D structures (Figure 5.21 (e)). In the case of the NAGAITIG peptide, self-assembled peptide fibrils are formed in solution but there is no peptide fibril formation on the functionalized structures. As soon

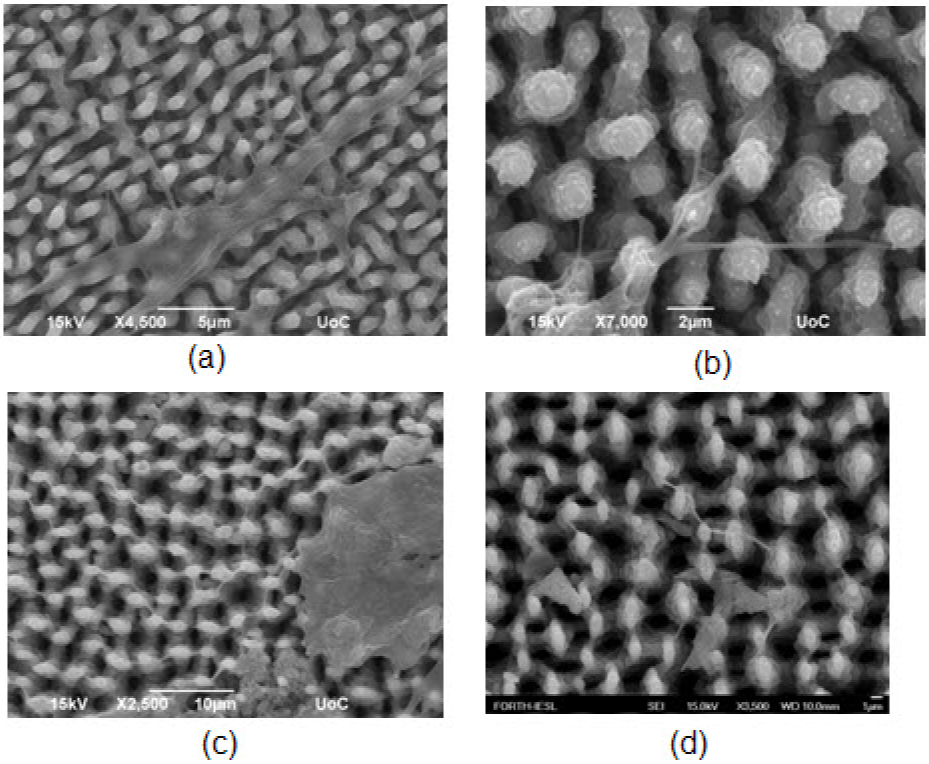

(a) (b) (c) (d)

Figure 5.20: SEM images of microstructured Si sample (with low roughness) coated with self-assembled NC fibrils.

as the peptide does not contain a cysteine residue to its sequence, there is no chemical bonding of the peptide fibrils on the surface and subsequently no bridges are formed.

At high roughness, a network of peptide fibrils is, also, formed (Figure 5.22 (a), (b) and (c)). The peptide fibrils engulf the the top of the Si cones (Figure 5.22 (b)) and peptide bridges are formed that link the tops of the microsrtuctures and, also, their bodies (Figure 5.22 (c)). Additionally, it is very interesting that two parallel bridges can be formed between two Si spikes (Figure 5.22 (a)).

From Figure 5.23 (a) and (b), we can observe the formation of the peptide bridges at higher magnification. For their formation, the existence of a thin layer of the peptide fibrils onto the Si microstructures is obviously necessary (Figure 5.23 (d), (e), (f) and (g)). Furthermore, the formation of a thin ”peptide sheet” is observed between two Si cones (Figure 5.23 (c)).

Finally, the network of the peptide fibrils is greatly extended and can reach up to 30-40 micrometers in length (Figure 5.24). Furthermore, it should be

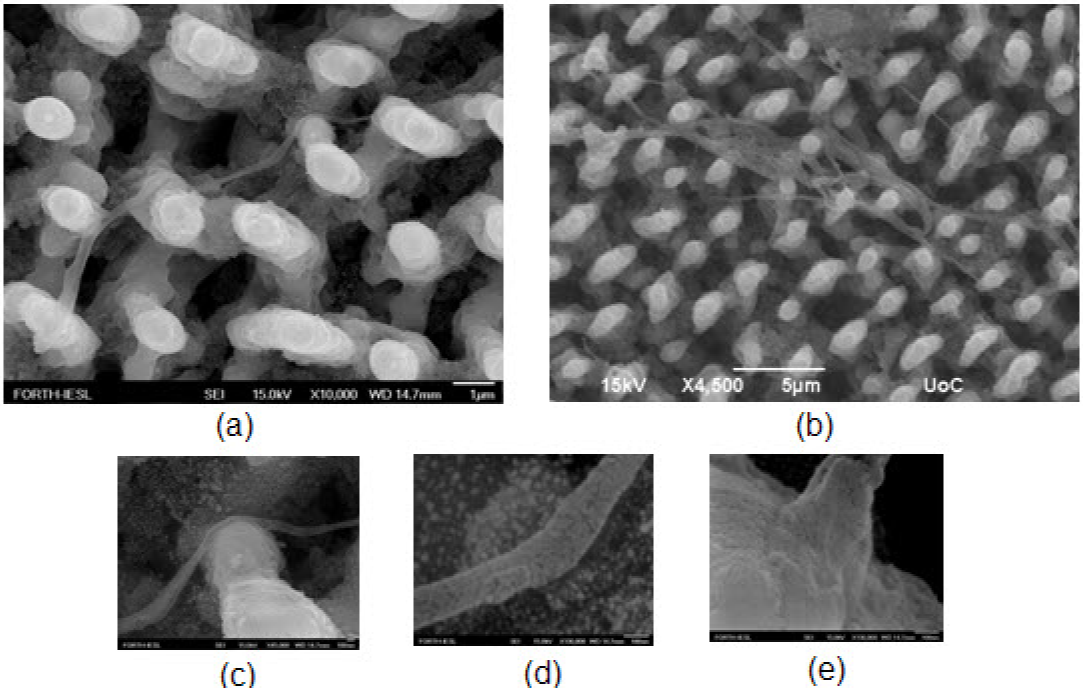

Figure 5.21: SEM images of microstructured Si sample (with mid roughness) coated with self-assembled NC fibrils.

noted that the microstructured, functionalized Si surface is not completely coated with the NC peptide fibrils, whereas, full peptide coverage of the NC peptides is observed onto the flat, functionalized Si.

5.3.5 Bioactive RGD-peptide

The modulation of the biological response of inorganic materials such as silicon could allow the design of more appropriate interfaces for implantable diagnostic and therapeutic silicon-based devices. Silicon-based implantable devices are of great interest due to silicon's availability and reproducibility, low-cost, and its integration ability in microelectronic applications. Surface modification of silicon substrates through adhesion of small biomolecules (peptides) or larger biomolecules (proteins) could enhance the biofunctionality of implanted biomedical devices.

More specifically, in the engineering of tissue growth, the extracellular matrix (ECM), which surrounds cells in a tissue, plays a pivotal role in the maintenance of cell phenotype and behavior. The fundamental role of the ECM

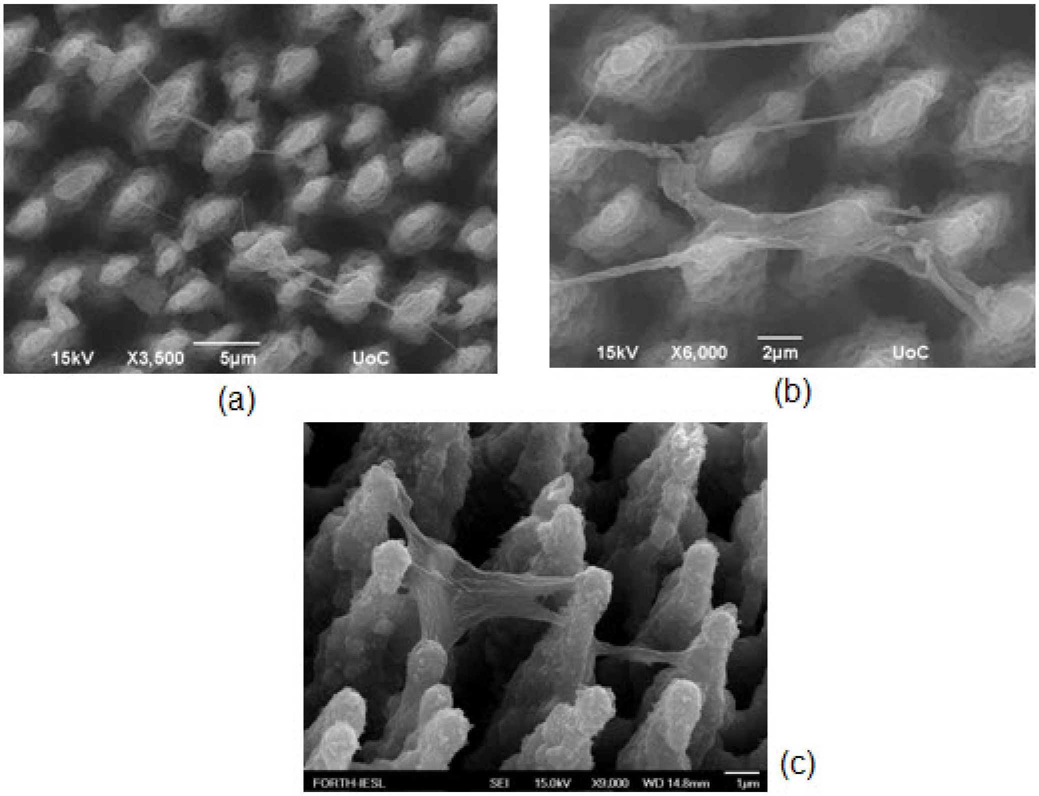

Figure 5.22: SEM images of microstructured Si sample (with high roughness) coated with self-assembled NC fibrils.

scaffold has led to structuring of material surfaces towards mimicking its features. As we have seen, ultrafast laser Si processing is a simple but an effective technique for the fabrication of three dimensional (3D) Si scaffolds with gradient roughness ratios and wettabilities. The modified surfaces, exhibiting controlled dual-scale roughness at both the micro- and the nano- scale, are subsequently used as culture substrates to facilitate cell seeding, adhesion and proliferation. The cell response to the micropatterned substrates depends on both physical and chemical properties, such as topography and surface energy, indicating that cell-surface interactions take place at multiple length scales and are subjected to variations of surface chemistry.

In particular, the ability of biomaterial surfaces to regulate cell behavior requires control over surface chemistry and microstructure. Cell attachment and cell growth are inherently affected by the microstructuring of silicon surfaces. However, one of the greatest challenges with silicon-based microdevices is the improvement of biocompatibility and tissue integration. This may be

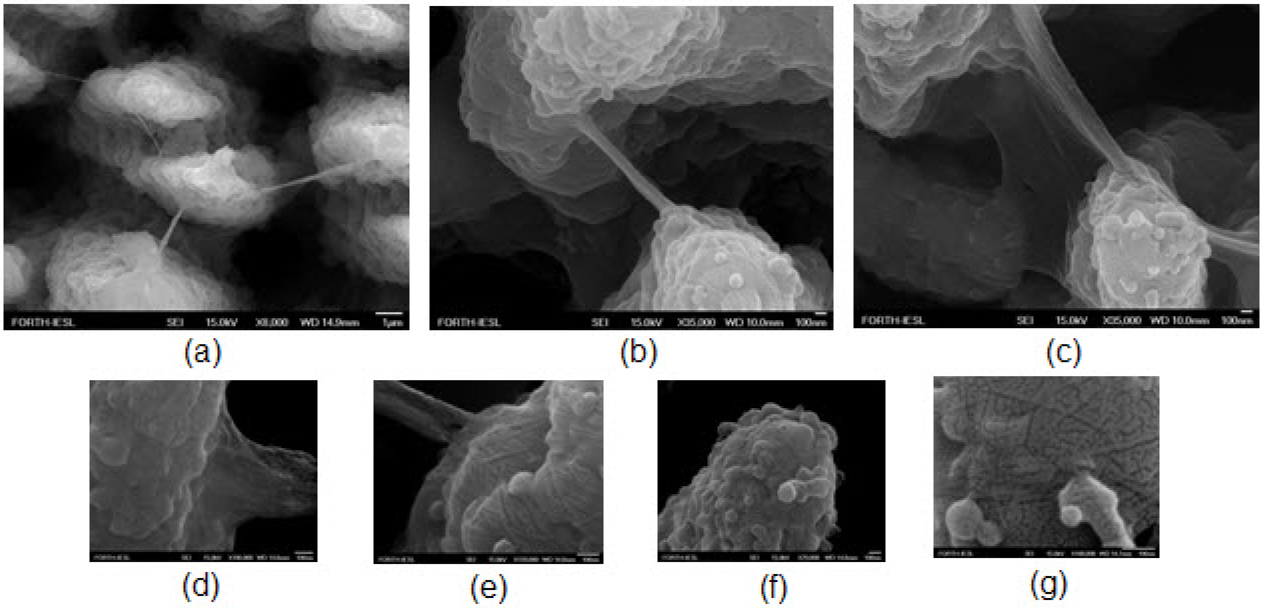

Figure 5.23: SEM images of microstructured Si sample (with high roughness) coated with self-assembled NC fibrils at higher magnification.

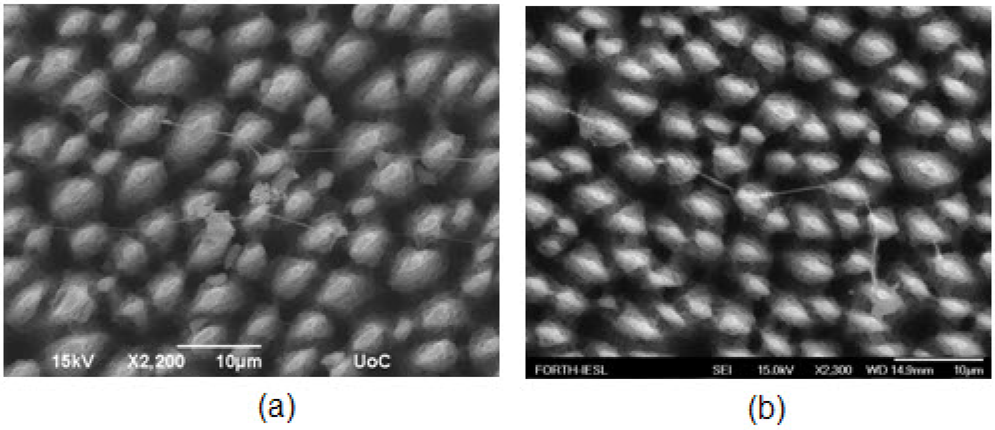

Figure 5.24: Top-view SEM images of microstructured Si sample coated with self-assembled NC fibrils

achieved by modified the exposed microstructured silicon surfaces with bioactive peptides. The RGD peptide can be used in order to alter the biological response of silicon substrates.

The cell adhesion factor RGD (or Arg-Gly-Asp) refers to the amino acid sequence containing argnine (R), glycine (G) and aspartic acid (D) side chains.

This peptide is involved in interactions between integrin proteins located in the cell membrane of most cells of the body and extracellular matrix proteins, such as fibronectin. It is expected that the immobilization of RGD peptide to the surface of materials can enhance adhesion of tissue forming cells. Integrins are heterodimeric cell surface receptors that were found in early studies to mediate adhesion cells and the extracellular matrix (ECM), by binding to ligands with an exposed arginine-glycineaspartate (RGD) sequence. These receptors also stimulate intracellular signaling and gene expression involved in cell growth, migration, and survival. Consequently, the impact of such bioactive peptides bound onto microstructured Si substrates on cell adhesion and growth should be thoroughly investigated.

Concluding Remarks

This dissertation has presented a method for inducing morphological modifications on the surface of Si upon ultrafast laser irradiation in reactive gas atmosphere or water environment. Such surface modifications can lead to changes in the optical and wetting properties of crystalline silicon. Si can be, also, altered to a great candidate for biological applications.

The main topics of this thesis are summarized below.

a) Increased optical absorptance

The use of laser structuring in reactive gas atmosphere (SF_6) or in water environment is a promising technique for improving the optical absorptance of Si. We have found that laser structuring in SF_6 improves the optical absorption substantially not only by increasing the absorptance in the wavelengths above the Si band-gap, but also at below-band gap wavelengths (>1100 nm), where crystalline Si does not normally absorb. Increasing the absorptance of Si up to more than 90% in the wavelength range of 250 nm$<\lambda<$2500 nm, gives the ability of using Si for applications related to detection of NIR wavelengths, which are specifically interesting for telecommunication applications and infrared imaging. Furthermore, upon laser processing in water the absorptance of nanostructured Si increases significantly and is about 95% in the wavelength range between 350nm and 1000nm.

b) Wetting response

Additionally, we have demonstrated that laser structuring in a reactive gas atmosphere or in water environment can be used for rendering the initially hydrophilic Si surface hydrophobic. This is a direct consequence of the morphology of the structured Si surfaces.

c) Biological applications

Finally, the adherence and viability of fibroblast cells on laser-structured Si surfaces has been investigated. It has been demonstrated that the patterned Si substrates can be potentially used as model scaffolds for the systematic exploration of the role of 3D micro/nano morphology and/or surface energy on cell adhesion and growth. We have, also, shown, a biofunctionalization technique in order to bind on microstructured Si surfaces amyloid peptides.

In summary, this thesis has shown that pulsed laser structuring in a reactive gas atmosphere or in aqueous environment is an efficient technique for improving the properties of Si, and extending its use into new types of application. Even though there are several scientific domains where laser-structured

Si may contribute to, we believe that we have provided insight to the potential use of Si as a biomaterial substrate in the field of tissue engineering.

Bibliography

[1] E.Jansen, R. Stedman, G.Grossman, H.G. Grimmeiss, Phys. Rev. B 29, 1907 (1984)

[2] J.F. Young,J .S. Preston,H .M. van Driel, and J.E. Siepe, Phys. Rev. B 27,1155 (1983)

[3] J.F.Young, J.E. Sipe, H.M. van Driel, Phys. Rev. B 30(4) , 2001 (1984)

[4] A. Smirl,T.F. Boggess,an d S. C. Moss,J . Appl. Phys. 60,1169 (1986)

[5] S. Ameer-Berg,W . Perrie, S. Rathbone,J. Wright, and W. Weaver,Appl. Surf. Sci. 127129,875 (1998)

[6] S. Nolte,C . Momma,H. Jacobs, A Tunnermann,B. N. Chikov, B. Wellegehausen, and H. Welling,J . Opt. Soc. Am. B 14,2716 (1997)

[7] D.von der Linde, K.Sokolowski-Tinten, J. Bialkowski, Appl. Surf. Sci. 109/110, 1 (1997)

[8] K. Sokolowski-Tinten,J . Bialkowski, M. Boing, A. Cavalleri,an d D. von der Linde, Phys. Rev. B 58,R 11 805 (1998)

[9] A. Cavalleri, K. Sokolowski-Tinten,J. Bialkowski,M . Schreiner, and D. von der Linde, J. Appl. Phys. 65,3301 (1999)

[10] E. Skantzakis, V. Zorba, D.G. Papazoglou, I. Zergioti, C. Fotakis Ultraviolet laser microstructuring of silicon and the effect of laser pulse duration on the surface morphology, Appl. Surf. Science 252, 4462 (2006)

[11] V. Zorba, Tailoring the Optical, Electronic and Wetting properties of Si surfaces by ultrafast laser microstructuring, Proc. of the 4th International WLT-Conference on Lasers in Manufacturing 2007

[12] B.N. Chikov, C. Momma,S. Nolte,a nd F. von Alvensleben, Appl. Phys. A 63,109 (1996)

[13] A.C. Tien, S. Backus, H. Kapteyn, M. Mourane, G. Mourou, Phys. Rev. Lett. 82, 3883 (1999)

[14] P.C.Becker, H.L.Fragnito, C.H.Brito Cruz, R.L. Fork, J.E. Cunningham, J.E.Henry, C.V.Shank, Phys. Rev. Lett. 61, 1647 (1988)

[15] S.I Dolgaev, S.V. Lavrishev, A.A. Lyalin, A.V. Simakin, V.V. Voronov, G.A. Shafeev, Appl. Phys. A 73, 177 (2001)

[16] J.E.Carey, C.H.Crouch, E.Mazur, Optics and Photonics News, 32, 2003

[17] D. Buerle, Laser Processing and Chemistry, Third Edition, Springer-Verlag Berlin Heidelberg New York (2000)

[18] K. Seeger and R.E. Palmer, Appl. Phys. Lett. 74,1627 (1999)

[19] R. Ortega Martinez,T .R. Verhey, P.K. Boyer,a nd J.J. Rocca, J. Vac. Sci. Technol.B 6,1581 (1988)

[20] F. Raksi, K. Wilson, Z. Jiang, A. Ikhlef, C.Y Cote, J. Kieffer, J. Chem. Phys.104, 6066 (1996)

[21] J.D.Fowlkes, A.J.Pedraza, D.H.Lowndes, Appl. Phys. Lett. 77, 1629 (2000)

[22] T.J. Chuang, J . Chem. Phys. 74, 1453 (1981)

[23] C.Wu, PhD thesis-Harvard (2001)

[24] F. Keliman, Phys. Rev. Lett. 51, 2079 (1983)

[25] S. Clark, D.C. Emmony, Phys. Rev. B. 40, 2031 (1989)

[26] M.Y. Shen, C.H. Crouch, J.E. Carey, R. Younkin, E. Mazur, M. Sheehy, C.M. Friend, Appl. Phys.Lett. 82(11), 1715 (2003)

[27] V. Zorba, PhD Thesis, 2007

[28] Mengyan Shen, James E. Carey, Catherine H. Crouch, Maria Candyla, Howard A. stone, and Eric Mazur, Nanoletters Vol.8, No.7, 2087-2091 (2008)

[29] C. H. Crouch, J. E. Carey, J. M. Warrender, M. J. Aziz, E. Mazur and F. Y. Genin Appl. Phys. Lett. 84 1850 (2004)

[30] C. H. Crouch, J. E. Carey, M.Y Shen, E. Mazur and F. Y. Genin Appl. Phys. A 79 1635 (2004)

[31] J. M. Palmer, Handbook of Optics (McGraw-Hill,1995)

[32] R. Menzel, Photonics: Linear and Nonlinear Interactions of Laser Light and Matter, .Springer-Verlag Berlin Heidelberg (2001)

[33] C.H. Seager,P .M. Lenahan, K. L. Brower, and R.E. Mikawa, J. Appl. Phys. 58, 2704(1985)

[34] W.B. Jackson,N .M. Johnson, D.K. Biegelsen, Appl. Phys. Lett. 43, 195 (1983)

[35] W.B. Jackson and N.M. Amer. Phys. Rev. B 25, 5559 (1982)

[36] A. Nakajima, A. Fujishima, K. Hashimoto, T. Watanabe, Adv. Mater. 11, 1365 1999)

[37] Z. Yoshimitsu, A. Nanajima, T. Watanabe, K. Hashimoto, Langmuir 18, 5818 (2002)

[38] N. A. Patankar Langmuir 19, 1249 (2003)

[39] W. Barthlott, C. Neinhuis, Planta 202, 1 (1997)

[40] J.-Y. Shiu, C.-W. Kuo, P. Chen C.-Y. Mou : Chem. Mater. 16, 561 (2004)

[41] P. N. Bartlett, J. J. Baumberg, P. R. Birkin, M. A. Ghanem, M. C. Netti: Chem. Mater. 14, 2199 (2002)

[42] I. Woodward, W. C. E. Schofield, V. Roucoules, J. P. S. Badyal: Langmuir 19, 3432 (2003)

[43] E. Martines, K. Seunarine, H. Morgan, N. Gadegaard, C. D. W. Wilkinson, M. O. Riehle: Nano Lett. 5, 2097 (2005)

[44] V. Zorba, L. Persano, D. Pisignano, A. Athanassiou, E. Stratakis, R Cingolani, P. Tzanetakis, C. Fotakis: Nanotechnology 17, 3234 (2006)

[45] N. S. Murthy, R. D. Prabhu, J. J. Martin, L. Zhou, , R. L Headrick.: J. Appl. Phys. 100, 023528 (2006)

[46] D. Buerle, Laser Processing and Chemistry, Third Edition, Springer-Verlag Berlin Heidelberg New York (2000)

[47] S. Clark, D.C. Emmony, Phys. Rev. B. 40, 2031 (1989)

[48] T. Baldacchini, J. E. Carey, M. Zhou, E. Mazur, Langmuir 22, 4917 (2006)

[49] P.G. De Gennes, Rev. Mod. Phys. 57, 827 (1985)

[50] L. Leger, J.F. Joanny, Rep. Prog. Phys. 55, 431 (1992)

[51] G. McHale, N.J. Shirtcliffe, M.I. Newton, Langmuir 20, 10146 (2004)

[52] R. N. Wenzel, Ind. Eng. Chem. 28, 988 (1936)

[53] A. B. D. Cassie, S. Baxter,Trans. Faraday. Soc., 40, 546 (1944)

[54] A. Marmur, Langmuir 19, 8343 (2003)

[55] A. Ulman, Chem. Rev. 96, 1533-1554 (1998)

[56] J.J. Gooding, F. Mearns, W. Yang and J. Liu, Electroanalysis 15, 81-96 (2003)

[57] N.K. Chaki, M. Aslam, J. Sharma and K. Vijayamohanan, Indian Acad. Sci. (Chem. Sci), 113, 659-670 (2001)

[58] J.B. Brzoska, I.B. Azouz and F. Rondelez, Langmuir 10, 4367-4373 (1994)

[59] S. Flink, F.C.J.M. van Veggel and D.N. Reinhoudt, J. Phys. Org. Chem. 14, 407-415 (2001)

[60] L.A. Chrisey, G.U. Lee and C.E. O'Ferrall, Nucleic Acids Research, 24, 3031-3039 (1996)

[61] J.A. Howarter, J.P. Youngblood, Langmuir 22 (2006) 11142

[62] P. Herder, L. Vgberg, P. Stenius, Colloids Surf. 34 (1988/1989) 117

[63] L.D. White, C.P. Tripp, J. Colloid Interface Sci. 232 (2000) 400

[64] A. Ebner, P. Hinterdorfer, H.J. Gruber, Ultramicroscopy 107 (2007) 922

[65] J. Kim, P. Seidler, L.S. Wan, C. Fill, Formation, structure, and reactivity of amino-terminated organic films on silicon substrates [2009]

[66] Y. Han, D. Mayer, A. Offenhausser, S. Ingebrant. Surface activation of thin silicon oxides by wet cleaning and silanization [2006]

[67] G. Arslan, M. Osmen, B. Gunduz, X. Zhang, M. Ersoz. Surface modification of glass beads with an aminosilane monolayer [2005]

[68] Self-assembled monolayers [Wikipedia]

[69] Dobson CM (2003) Protein folding and misfolding

[70] Dobson CM (1999), Protein misfolding, evolution and disease, TRENDS IN BIOCHEMICAL SCIENCES 24 (9): 329-332

[71] Papanikolopoulou K, Schoehn G, Forge V, Forsyth VT, Riekel C, Hernandez JF, Ruigrok RWH, Mitraki A (2005), Amyloid fibril formation from sequences of a natural beta-structured fibrous protein, the adenovirus fibril JOURNAL OF BIOLOGICAL CHEMISTRY 280 (4): 2481-2490

[72] Emmanouil Kasotakis, Master Thesis Design and study of composite biomaterials based on self-assembling peptides from natural fibrous proteins [2008]

[73] Martin Stutzmann*, Jose Antonio Garrido, Martin Eickhoff, and Martin S. Brandt, Direct biofunctionalization of semiconductors: A survey [2006]

[74] Causa F, Netti PA, Ambrosio L. A multi-functional scaffold for tissue regeneration: the need to engineer a tissue analogue. Biomaterials 2007;28:5093

[75] Falconnet D, Csucs G, Grandin HM, Textor M. Surface engineering approaches to micropattern surfaces for cell-based assays. Biomaterials 2006;27:3044.

[76] Hutmacher DW. Scaffolds in tissue engineering bone and cartilage. Biomaterials 2000;21:2529

[77] Cen L, Liu W, Cui L, Zhang WJ, Cao YL. Collagen tissue engineering: development of novel biomaterials and applications. Pediatric Res 2008;63:492

[78] Kurella A, Dahotre NB. Review paper: surface modification for bioimplants: the role of laser surface engineering. J Biomater Appl 2005;20:5.

[79] Stevens MM, George JH. Exploring and engineering the cell surface interface. Science 2005;310:1135.

[80] Cyster LA, Parker KG, Parker TL, Grant DM. The effect of surface chemistry and nanotopography of titanium nitride (TiN) films on 3T3-L1 fibroblasts. J Biomed Mater Res Part A 2003;67A:138.

[81] Cyster LA, Parker KG, Parker TL, Grant DM. The effect of surface chemistry and nanotopography of titanium nitride (TiN) films on primary hippocampal neurones. Biomaterials 2004;25:97.

[82] Backman L. Shape changes of the human red-cell studied by aqueous 2-phase partition. Febs Lett 1990;262:107.

[83] Salloum DS, Olenych SG, Keller TCS, Schlenoff JB. Vascular smooth muscle cells on polyelectrolyte multilayers: hydrophobicity-directed adhesion and growth. Biomacromolecules 2005;6:161.

[84] Flemming RG, Murphy CJ, Abrams GA, Goodman SL, Nealey PF. Effects of synthetic micro- and nano-structured surfaces on cell behavior. Biomaterials 1999;20:573.

[85] Reichert J, Brukner S, Bartelt H, Jandt KD. Tuning cell adhesion on PTFE surfaces by laser induced microstructures. Adv Eng Mater 2007;9:1104.

[86] Stratakis E, Ranella A, Farsari M, Fotakis C. Laser based micro/nanoengineering for biological applications. Progr Quant Electron 2009;33:127.

[87] Grinnell F. Cellular adhesiveness and extracellular substrate. Int Rev Cytol 1978:65.

[88] Reinhardt C, Passinger S, Zorba V, Chichkov BN, Fotakis C. Replica molding of picosecond laser fabricated Si microstructures. Appl Phys A-Mater Sci Process 2007;87:673.

[89] Oner D, McCarthy TJ. Ultrahydrophobic surfaces. Effects of topography length scales on wettability. Langmuir 2000;16:7777.

[90] Charest JL, Garcia AJ, King WP. Myoblast alignment and differentiation on cell culture substrates with microscale topography and model chemistries. Biomaterials 2007;28:2202.

[91] Dalby MJ, Riehle MO, Sutherland DS, Agheli H, Curtis ASG. Changes in fibroblast morphology in response to nano-columns produced by colloidal lithography. Biomaterials 2004;25:5415.

[92] Ingber DE. Cellular tensegrity: defining new rules of biological design that govern the cytoskeleton. J Cell Sci 1993;104:613.

[93] Andersson AS, Backhed F, von Euler A, Richter-Dahlfors A, Sutherland D, Kasemo B. Nanoscale features influence epithelial cell morphology and cytokine production. Biomaterials 2003;24:3427.